

AD-A044 836

ENVIRONMENTAL RESEARCH INST OF MICHIGAN ANN ARBOR

F/G 14/5

BASIC REMOTE SENSING INVESTIGATION FOR BEACH RECONNAISSANCE.(U)

SEP 77 D LYZENGA, R SHUCHMAN, F THOMSON

N00014-74-C-0273

UNCLASSIFIED

ERIM-108900-9-P

NL

| OF |  
AD  
A044836



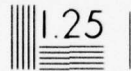
END  
DATE  
FILMED  
10-77  
DDC



1.0



1.1



1.25



2.8

3.2

3.6

4.0



2.5



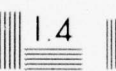
2.2



2.0



1.8



1.4



1.6

MICROCOPY RESOLUTION TEST CHART  
NATIONAL BUREAU OF STANDARDS-1963-A

AD A 044 836

12  
b.s.

Interim Progress Report

# BASIC REMOTE SENSING INVESTIGATION FOR BEACH RECONNAISSANCE

D. LYZENG, R. SHUCHMAN, F. THOMSON,  
C. F. DAVIS, G. H. SUITS

SEPTEMBER 1977

Approved For Public Release; Distribution Unlimited

DDC  
OCT 4 1977  
C

Prepared for:  
Geography Branch  
Office of Naval Research  
Arlington, VA 22217  
Contract No. N0014-74-C-0273

AD No. \_\_\_\_\_  
DDC FILE COPY

ENVIRONMENTAL  
**RESEARCH INSTITUTE OF MICHIGAN**  
FORMERLY WILLOW RUN LABORATORIES, THE UNIVERSITY OF MICHIGAN  
BOX 618 • ANN ARBOR • MICHIGAN 48107

# NOTICES

Sponsorship. The work reported herein was conducted by the Environmental Research Institute of Michigan for the Geography Branch, Office of Naval Research, Arlington, Virginia, 22217, Contract No. N0014-74-C-0273. Contracts and grants to the Institute for the support of sponsored research are administered through the Office of Contracts Administration.

Distribution. Initial distribution is indicated at the end of this document.

DDC Availability. Qualified requesters may obtain copies of this document from:

Defense Documentation Center  
Cameron Station  
Arlington, Virginia 22314

Final Disposition. After this document has served its purpose, it may be destroyed. Please do not return it to the Environmental Research Institute of Michigan.

ACCESSION for	
NTIS	White Section <input checked="" type="checkbox"/>
DDC	Buff Section <input type="checkbox"/>
UNANNOUNCED	<input type="checkbox"/>
JUSTIFICATION	
BY	
DISTRIBUTION/AVAILABILITY CODES	
Dist.	SP-CIAL
A	

14

SECURITY CLASSIFICATION OF THIS PAGE (When Data Entered)

REPORT DOCUMENTATION PAGE

READ INSTRUCTIONS  
BEFORE COMPLETING FORM

ERIM

1. REPORT NUMBER

108900-9-P

2. GOVT ACCESSION NO.

3. RECIPIENT'S CATALOG NUMBER

4. TITLE (and Subtitle)

Interim Report, BASIC REMOTE SENSING INVESTIGATION FOR  
BEACH RECONNAISSANCE

5. TYPE OF REPORT & PERIOD COVERED

Interim Report, 1 Jan - 31 Dec 76

6. PERFORMING ORG. REPORT NUMBER

108900-9-P

8. CONTRACT OR GRANT NUMBER(s)

N0014-74-C-0273

7. AUTHOR(s)

D. Lyzenga, R. Shuchman, F. Thomson, C.F. Davis, G.H. Suits

9. PERFORMING ORGANIZATION NAME AND ADDRESS

Environmental Research Institute of Michigan  
Post Office Box 618  
Ann Arbor, Michigan 48107

10. PROGRAM ELEMENT PROJECT TASK  
AREA & WORK UNIT NUMBERS

11. CONTROLLING OFFICE NAME AND ADDRESS

Geography Branch  
Office of Naval Research  
Arlington, Virginia 22217

12. REPORT DATE

September 1977

13. NUMBER OF PAGES

70 Text + 7 Preliminary

14. MONITORING AGENCY NAME AND ADDRESS  
(if different from Controlling Office)

15. SECURITY CLASS (of this report)

Unclassified

15a. DECLASSIFICATION/DOWNGRADING  
SCHEDULE

16. DISTRIBUTION STATEMENT (of this Report)

Distribution of this document is unlimited.

17. DISTRIBUTION STATEMENT (of the abstract entered in Block 20, if different from Report)

13 N0014-74-C-0273

18. SUPPLEMENTARY NOTES

19. KEY WORDS (Continue on reverse side if necessary and identify by block number)

Beach Reconnaissance  
Remote Sensing  
Multispectral Scanner  
Data Processing  
Multifrequency Synthetic Aperture Radar

20. ABSTRACT (Continue on reverse side if necessary and identify by block number)

Progress is reported on two tasks designed to develop remote sensing beach reconnaissance techniques applicable to benthic and beach intertidal zones. In Task 1, whose goal is to develop remote sensing algorithms for important beach composition and physical parameters, results of radiative transfer model development and application are reported. The model calculates the radiance of a beach, given physical and compositional information. In Task 2, whose goal is to develop remote sensing algorithms for mapping of bottom features in the benthic zone, results of radiative transfer model calculations and an evaluation of the modified ratio algorithm (MRA) performance in scattering waters are presented.

407743

JP

## TABLE OF CONTENTS

	Page
1. INTRODUCTION AND SUMMARY . . . . .	1
1.1 Description of Tasks . . . . .	1
1.1.1 Beach Environment Tasks . . . . .	1
1.1.2 Bottom Features Mapping Task . . . . .	2
1.2 Summary of Results . . . . .	4
2. POTENTIAL USE OF ONR FUNDED DEVELOPMENTS IN OTHER PROGRAMS.7	
2.1 Underwater Features Mapping Payoff . . . . .	7
2.2 Beach Environment Payoff . . . . .	8
3. BEACH ENVIRONMENT STUDY . . . . .	9
3.1 Approach . . . . .	9
3.2 Modeling . . . . .	12
3.2.1 Introduction . . . . .	12
3.2.2 Reflectance Model Concepts . . . . .	12
3.2.3 Optical Properties of Sand Components . . . . .	15
3.3.4 Model Software Description . . . . .	19
3.3.5 Preliminary Modeling Results . . . . .	24
3.3 Assessment of Radiation Penetration in Beach Sands	27
3.3.1 Rationale . . . . .	27
3.3.2 Description of Skin Depth Measurements . . . . .	27
3.3.3 Results of Skin Depth Measurements . . . . .	29
3.4 Plans for Future Beach Environment Task Work . . . . .	31
4. UNDERWATER FEATURES STUDY . . . . .	33
4.1 Model Development . . . . .	33
4.2 Parameter Selection and Model Results . . . . .	35
4.3 Description of MRA Technique . . . . .	40
4.4 Evaluation of MRA Technique . . . . .	46
4.5 Further Algorithm Development . . . . .	54
APPENDIX A: DESCRIPTION OF ONR DEVELOPED BEACH ENVIRONMENT COMPUTER PROGRAMS INCLUDING SAMPLE OUTPUT . . . . .	57
A.1 Description of Programs . . . . .	58
A.1.1 ABSCAT . . . . .	58
A.1.2 PREDICT . . . . .	59
A.1.3 OPAQUE . . . . .	59
A.1.4 STAIN . . . . .	60
A.1.5 SANDREF . . . . .	60
REFERENCES . . . . .	68
DISTRIBUTION LIST . . . . .	69

## LIST OF FIGURES

	Page
1. Cross Section of Sand Layers . . . . .	16
2. Model Flow . . . . .	21
3. Comparison with Measured Carbonate Reflectance to SANDREF Model Result . . . . .	26
4. Comparison with Measured Quartz Reflectance to SANDREF Model Result . . . . .	26
5. Skin Depth Measuring Apparatus . . . . .	28
6. Irradiance Attenuation Coefficients for Jerlov's Water Types 1, 3 and 5 . . . . .	37
7. Volume Scattering Functions vs. Scattering Angle for Petzold's Stations 9, 5 and 2200 . . . . .	38
8. Spectral Reflectance of Sand, Mud and Green Vegetation	39
9. Two-Channel Plot of Radiances over Water Type 5 . . .	41
10. Two-Channel Plot of Radiances over Water Type 3 . . .	42
11. Two-Channel Plot of Data Values from St. Andrew Bay, Florida Curves Indicate Trajectories Calculated for Sand (Lower Curve) and Vegetation (Upper Curve) . . . . .	43
12. Illustration of Modified Ratio Algorithm . . . . .	44
13. Probability of Misclassification vs. Depth for Water Type 3 . . . . .	49
14. Probability of Misclassification for Vegetation vs. Depth in Three Situations . . . . .	50
15. Average Probability of Misclassification for Three Bottom Types vs. Depth in Three Situations . . . . .	51
16. Log-Log Plot of Bottom Reflectance Signals for Water Type 5 at .475 $\mu\text{m}$ and .525 $\mu\text{m}$ . . . . .	55

## LIST OF TABLES

	<u>Page</u>
1. Common Beach Forming Materials . . . . .	20
2. Results of Empirical Skin Depth Measurements . . . . .	30
3. Summary of MRA Performance . . . . .	53
A.1. SANDREF Input Parameter Definitions . . . . .	61
A.2. Example of SANDREF Input File . . . . .	62

## ACKNOWLEDGMENTS

This work was the combined effort of a number of ERIM staff members. In the Beach Environment Task, under the direction of Robert Shuchman, basic mathematical modelling assistance was provided by Dr. Gwynn Suits. Abby Liskow contributed mineralogical information on the common beach minerals. Lewis Munford made Cary 14 spectrophotometer measurements. Carl Davis assisted in the spectrophotometer data reduction and in the study of skin-depth effects. Dave Franczak provided computer programming expertise.

In the Underwater Features Task, under the direction of Dr. David Lyzenga, Elaine Marinello provided analytical assistance. The assistance of Marcia Martilotti and Nancy Moon in report preparation is also acknowledged.

## INTRODUCTION AND SUMMARY

This interim report on contract N0014-74-C-0273 summarizes work on two tasks comprising the third year's effort. The work was accomplished by various task leaders at the Environmental Research Institute of Michigan under the overall guidance of Principal Investigator Fred Thomson. The performance period for the work reported herein was January 1976 - December 1976.

This introduction contains a description of tasks and a discussion of their relevance to the beach reconnaissance problem, a summary of progress to date on each task, and recommendations for future work. The introduction is followed by detailed technical discussions of work on each task.

## 1.1 DESCRIPTION OF TASKS

Effort on two tasks was continued in the third year of the contract. The purpose of each task was to build on a proven capability for mapping features pertinent to beach reconnaissance using remote sensing technology and to develop new or refined information extraction capabilities. These capabilities will yield new or better beach reconnaissance information from remote sensing data.

## 1.1.1 BEACH ENVIRONMENT TASK

The Beach Environment Task (leader, Robert Shuchman) is built from the proven capability of mapping silicate minerals using reststrahlen techniques developed by Vincent and Thomson [1]. In previous years, a data base of the spectral directional reflectance of fifty diverse silica beach samples was assembled, some reflectance data in the 3-14  $\mu\text{m}$  spectral range was obtained, and empirical analysis of the spectra resulted in several algorithms which showed high correlation between linear sums of wavelength-averaged reflectance

and of reflectance ratios and important beach physical properties such as moisture content, grain size, and degree of sorting. Analysis of the 3-14  $\mu\text{m}$  data revealed the extent to which compositional differences could be distinguished from changes in the silicate reststrahlen bands in the 8-10  $\mu\text{m}$  range.

But the measurement of more reflectance spectra of beach sands in order to verify the utility and generality of the algorithms developed by empirical analysis seemed 1) too costly, 2) not very complete, as results would be dependent on the spectra in the data base, and 3) not conducive to an understanding of the physical processes which cause the reflection of light from beaches.

Consequently, radiative transfer models of Gwynn Suits [2] were adapted (under ERIM internal funding) to calculate the reflectance of beach sand. Supportive measurements necessary to obtain the data needed for input to Suit's model were carried out under contract funding. Model calculations of the reflectance of a carbonate and a silicate beach sand were made and results are reported in detail in section 2 and summarized in section 1.2

#### 1.1.2 BOTTOM FEATURES MAPPING TASK

The Bottom Features Mapping Task (leader, Dr. David Lyzenga) is built from a proven capability of water depth mapping using the selective penetration of water in various spectral bands sensed by a passive multispectral scanner. Last year we defined suitable spectral bands, defined the depth penetration capability of the modified ratio algorithm (MRA), and began to determine which types of bottom features were discriminable, assuming non-scattering waters. Also, a model was developed for calculating the radiance from shallow scattering waters where the reflected energy from the bottom constitutes a major portion of the observed radiance.

This year, the radiative transfer model was exercised to calculate the spectral radiance of three different bottom types, in three different

types of water, for a number of different wavelengths. Then the performance of the MRA was evaluated by drawing decision boundaries optimally separating the three bottom types at a "training depth", and computing the probability of misclassification at other depths. Results are presented and discussed in section 3, and summarized in section 1.2.

## 1.2 SUMMARY OF RESULTS

In the Beach Environment Task, the following accomplishments were made this year:

1. A model was developed (from a vegetation canopy reflectance model of G. Suits) to calculate the reflectance of beach samples, given the composition of the sample, some optical properties of the constituents, and a knowledge of the beach moisture profile (on a millimeter scale).
2. Because the fundamental optical properties of beach constituents were not available, a program was completed to measure the optical properties. Spectral absorption and scattering coefficients and the forward scattering fraction were measured for 16 common beach-forming minerals over the range 0.4-2.2  $\mu\text{m}$ .
3. To provide knowledge of the millimeter scale moisture variations in beaches, some field studies were initiated after it was found that adequate information did not exist in the literature.
4. Preliminary model calculations of spectral reflectance show good agreement with the measured values of reflectance for the same beach samples. A more thorough evaluation of the model calculations will be performed before using the calculated radiance values for multispectral algorithm development.
5. The preliminary model calculations show the importance of iron stain and opaque minerals in controlling the reflectance of predominantly quartz beaches. This occurs because quartz is a very transparent material and the dominant effect of the quartz is to scatter the radiation. Because of the scattering, radiation has a greater chance to be absorbed by stain or opaque particles.

In the Underwater Features Task, the following conclusions were reached:

1. An evaluation of the modified ratio algorithm (MRA) was conducted using a radiative transfer model previously developed. Effects of changes in wavelengths selected, changing water type, and changing deep water offset signal on the probability of misclassification of vegetation, sand, and mud bottom types were assessed.

Changes in water type degrade the performance of MRA, by reducing the range of depths over which adequate performance can be obtained. For example, using an algorithm optimized for Jerlov Type 3 water and deep water offsets from Type 1 water, 50% or better average probability of misclassification can be obtained out to 6 m water depth. The same algorithm operating in Type 5 water achieves this performance only out to 3.6 m depth.

2. Changes in deep water offset signal from that appropriate for the water type degrade performance at shallow water depths but may actually improve performance at large water depths.
3. The major limitation to the MRA technique is that two wavelengths must be chosen such that the water attenuation coefficient is the same in each band. This, coupled with the need to select wavelengths which penetrate the water, leads to low target to target contrast and consequently sub-optimum performance for targets of interest (e.g., sand, mud and vegetation). The reflectance ratios of these materials are quite similar in the bands selected. For example, the average probability of misclassification among the three targets selected, at zero water depth was 13.2, 16.6, and 26.7% for wavelength pairs selected for water types 1, 3, and 5 respectively. This is marginally acceptable performance. At zero water depth, this performance is only attributable to the selection of bands.

4. There are more promising algorithms, not involving the ratio technique, and not subject to the requirement that wavelengths must be chosen where water attenuation coefficients are equal. The performance of these algorithms should be investigated.

## POTENTIAL USE OF ONR FUNDED DEVELOPMENTS IN OTHER PROGRAMS

Although the present Underwater Features Mapping Task and Beach Environment Task are making important contributions to basic remote sensing, we wish to note that the developments which we are making are also potentially of use in on-going 6.2 programs of the U.S. Navy and in programs of other government agencies. Some of the anticipated or potential applications of these techniques are discussed below.

## 2.1 Underwater Features Mapping Payoff

We are aware of several programs in coastal ecology, bathymetry surveying and in Offshore Continental Shelf assessment where we feel that the techniques we are developing under the Underwater Features Task could be applied. In coastal ecology, a NOAA program to map benthic algal communities in Alaska could benefit. Present surveys (performed by ERIM in the summer of 1976) were made at low tide, necessitating careful scheduling around tide and weather conditions. In Alaska, the available flight time because of these constraints can be very small. Being able to map algal communities while submerged will offer greater operational flexibility. Additionally, the techniques would be helpful in assessing the situation of oyster habitat in Florida, which we know is of some interest to EPA.

One of the most important uses of the underwater features mapping capability is in extending bathymetry calibration points (obtained by pulsed laser) to calibrate passive multispectral bathymetry algorithms. Such techniques are of great interest to the U.S. Navy for Tactical Beach Reconnaissance. ERIM is currently engaged in a multiyear program of developing a breadboard Beach Reconnaissance sensor/processor package, under funding from the Naval Coastal System Laboratory (Contract N61339-77-C-C059).

Last, with the increased pressure to develop offshore oil reserves of the U.S., the Bureau of Land Management has been charged with the responsibility to survey offshore Continental Shelf areas to assess the environmental impact of offshore oil drilling, pipeline construction, and shore processing facilities. The underwater features mapping algorithms, when perfected, will serve as a useful tool for mapping nearshore features.

## 2.2 Beach Environment Payoff

The algorithms for determining important beach parameters (composition, grain size, degree of sorting) from remotely sensed data will be useful in addition to providing basic understanding of beach formation and dynamics. Information obtained can be used in trafficability/mobility models developed by the U.S. Army Corps of Engineers Waterways Experiment Stations (Vicksburg). The trafficability/mobility models in turn provide information essential to the Navy and Marine Corps for Beach Reconnaissance operations.

Two other applications of the beach algorithms might be in the location of heavy minerals on beaches. This is important to companies mining heavy minerals. For example, a large amount of titanium is obtained from beach deposits in North Carolina. Certain rare earth minerals are also present in these deposits. Also, by mapping grain size distributions on beaches, some important information might be obtained on energy inputs to beaches.

## BEACH ENVIRONMENT STUDY

## 3.1 APPROACH

The present effort began in 1974. During the first two years, 50 beach samples from a broad range of environments were collected. The physical and chemical characteristics and the spectral reflectance in the visible, near infrared, and thermal infrared spectral regions were measured. Analyses of these measurements demonstrated correlations between spectral reflectance features and certain chemical and physical properties, and stimulated efforts to develop a theoretical model to explain these correlations. Later this data will prove valuable as a test set for verification of this model.

Specifically in the first two years of beach environment ONR work [1], we have observed:

- (1) that near infrared (0.8-1.8  $\mu\text{m}$ ) reflectance of beach samples decreases monotonically with moisture content by volume. There are some residual effects of grain size such that if the sample universe is stratified into coarse (grain size  $>1$  mm) and fine (grain size  $<1$  mm) the correlation between moisture content and reflectance improves. Sample composition, for typical quartz, quartz-feldspar, and some heavy mineral beaches, apparently plays a minimal role in determining near infrared reflectance.
- (2) The quartz reststrahlen features at 8-10  $\mu\text{m}$  are reliable indicators of quartz, more or less independently of moisture content (from 0-24% by volume) and grain size (from 0.33-2 mm mean grain size). The magnitude of the reststrahlen feature, measured in reflectance, is proportional to the percentage of quartz in a sample. Concentrations of 10-15% feldspar and kaolinite can be discriminated in the reststrahlen features as a broadening of the reflectance feature, particularly

at the longer (10-11  $\mu$ m) wavelengths. Smaller (3-5%) concentrations of heavy minerals can also be discerned in the spectra as a variation in the reflectance in the 10-12  $\mu$ m region, beyond the quartz reststrahlen bands.

- (3) While computer statistically selected single band and band ratio models (bands in the visible and near infrared) seem to predict grain size with a high degree of confidence, there did not appear to be a rational physical justification of the bands or band ratios selected.

The current effort was directed toward explaining the correlations which we observed in the analysis of measured reflectance data. To accomplish this, we developed theoretical modelling techniques to compute the spectral reflectance of beach sands, given the spectral properties of the constituents, the composition of the beach sand, and the moisture profile of the beach sand. Initially, we felt that a number of these parameters would be available from literature, and we could exercise the developed models to verify and improve the algorithms developed in previous work. However, careful literature review revealed that the required data on optical parameters of beach-forming minerals and the moisture profile of beaches (on a scale of millimeters) did not exist. These data were obtained as part of this year's effort, and they represent a substantial contribution to the knowledge of the optical properties of beach-forming minerals and of the moisture profiles of beaches. But as a result of the need to measure this basic information, the model exercise was not begun until late in the year, and that work is not complete.

The GCANOPY and AQUACAN (leaf reflectance) models for Dr. G. Suits [2] were adapted to calculate reflectances of beach sands.\*

---

\*The adaptation of the Suits' models to the ONR effort was accomplished under ERIM IR&D funds. Dr. Suits consultation time on various aspects of the adaption of his model were also covered by IR&D funds.

The adapted Suits' models (called SANDREF and AQUASANDREF) will be used to determine the practical limits of remote sensing algorithms for determining physical and chemical properties of beaches. The new models need the coefficients of absorption and scattering and the forward scattering fraction for each mineral comprising the beach sand (i.e., quartz, feldspar, kaolinite, etc), the average number of grains (particles) per given volume from which average cross sections of each mineral type can be computed, and the moisture depth profile of the beach to calculate the reflectance of the beach. ERIM using its Cary 14 spectral reflectometer, measured the hemispherical transmittance and reflectance of each beach forming mineral at a number of prescribed thicknesses to obtain the needed coefficients and forward scattering fraction. The measurements of the fundamental optical properties of common beach forming minerals in the 0.4-2.2  $\mu\text{m}$  range of the electromagnetic spectrum are the first such measurements reported to be made. The results of this phase of the work are currently being prepared for journal publication, and are further discussed in Section 2.2.

To obtain moisture depth profiles of typical beaches on a millimeter scale, ERIM initiated a careful search of the literature and consulted various experts in the field of soil moisture as to the availability of this information. Like the needed optical properties of minerals, the moisture data at the millimeter profiling scale was not available. ERIM developed a measuring apparatus to obtain the moisture data for use in the AQUACAN model. In situ field measurements (along Lake Huron) and laboratory measurements were made to obtain volume of water as a function of depth from the top of the sand surface. The laboratory measurements utilized beach samples that were previously collected, dried and then wetted to simulate actual beach conditions. These derived moisture profile information was used in the AQUASANDREF model.

A laboratory apparatus was also developed to empirically measure the "skin depth" of passive multispectral techniques. The empirically obtained skin depth measurements were compared to one preliminary "skin depth" result obtained using the SANDREF model. The results were within  $\pm 1$  mm in 10 mm agreement. Those results are discussed in section 2.3.

### 3.2 MODELING

#### 3.2.1 INTRODUCTION

The capability for determining important physical properties of beach sands by remote sensing techniques depends upon the interaction of radiation with the constituent materials of the beach. Such interaction is certainly complex but, nevertheless, must follow the laws of nature. The purpose of making a mathematical reflectance model of this complex interaction is to achieve insight into the relationship between the remotely received signals and the physical properties of the beach sand that are of interest.

A mathematical model of a physical phenomenon is the result of incorporating the mathematical expressions of the laws of nature as they apply to a complex circumstance so that the conclusions drawn from the assembled expressions correspond to the physical results of an experiment under similar circumstances. Such a model requires experimental validation using a few but diverse circumstances in order to prove that the essence of the phenomenon is contained in the logic of the model. Once validation has been achieved, the model may be used as a readily available and inexpensive substitute for experiment under all circumstances within the scope of the circumstances of the validation experiments. In addition, the logical structure of the model provides the insight into the significant interaction processes so that more general conclusions may be drawn.

#### 3.2.2 REFLECTANCE MODEL CONCEPTS

The most elementary model of sand reflectance is the simple plane mixtures model. The model employs the assumptions that all sand particles are opaque and are randomly mixed. The surface of the sand layer exposes sand particles in proportion to the product of their mean cross sectional area and the concentration of the particles in the sand mixture. Thus, the reflectance spectrum of the mixture is predicted to be the area weighted average of the reflectance spectra of

the various minerals exposed at the sand surface. Multiple scattering between particles is assumed to be negligible and one surface particle is assumed not to obscure from view an adjacent surface particle.

This elementary model fails to achieve good accuracy because the transmittance of particles in a finely divided state may be quite large and multiple scattering of radiation between particles should be significant. In addition, the packing of grains in layers produces partial exposure at the surface so that line of sight to some particles will depend upon the direction of view. A more complex model is required to account for these effects.

The more complex model which is used in this work employs the identical concepts that are employed by the directional reflectance model for vegetative canopies [2]. It may be hard to visualize off-hand that the interaction of radiation with a vegetative canopy is homomorphic with the interaction of radiation with sands because vegetation and sand hardly appear the same to the eye. Nevertheless, the essence of the reflection, transmission, and multiple scattering phenomena is the same except for the optical parameters of the components that are involved as long as the wavelength is much smaller than the particles.

The first assumption of this model is that the scattering components are distributed more or less uniformly in horizontal layers where the mixture of component types may be different in the various layers. In a corn field, for example, the tassels always appear at the top, green healthy mature leaves appear in a middle layer and necrotic leaves appear usually near the soil. In sands, the action of wind and waves are likely to stratify mineral mixtures vertically and certainly moisture content varies with a vertical moisture profile. The division in layers is done in order to quantize statistically what may otherwise be nearly a continuous distribution.

The second assumption is that the radiation field may be divided into two types of radiant flux -- specular and diffuse. The specular

flux represents the radiation arriving from the source with rectilinear propagation and passes through the holes, cracks, and voids of the ensemble of randomly packed components without deviation. The diffuse flux is derived from the specular flux and is that part of the specular flux which has been intercepted by a scattering component at least once and is scattered in both forward and backward directions. In a vegetative canopy, specular flux frequently reaches the soil level and appears as sun flecks on the soil. In a sand, specular flux diminishes exponentially to negligible proportions in only a few millimeters depth. Optically, the sand is infinitely deep. However, the diffuse flux is derived from the specular flux in the identical manner. The diffuse flux may penetrate much deeper into the sand than can specular flux.

The third model assumption is that the manner of scattering by mineral particulates can be adequately represented by replacing each mineral particulate with a set of equivalent Lambertian panels which have the same spectral transmittance and reflectance as does the component. This assumption defines a simplified scattering phase function which permits one to calculate ensemble reflectances in closed form. The form of the scattering phase function becomes significant when single scattering is the dominant phenomenon. Scattering by widely dispersed aerosols in the atmosphere (e.g., smoke and dust) exhibits detailed phase function effects. However, as the degree of multiple scattering increases, the detailed features of the scattering phase function are no longer significant. In both sands and vegetative canopies, multiple scattering effects dominate because of the high density of scattering components.

The fourth model assumption is that the diffuse flux moves generally vertically upward and downward with a Lambertian angular distribution as a first approximation. The reflectance of the ensemble is calculated using the method of self-consistent field with the specular and approximate diffuse flux as the illuminant of components. The ensemble reflectance is not necessarily Lambertian but is only approximately so. Both vegetation and sand meet this approximate criterion.

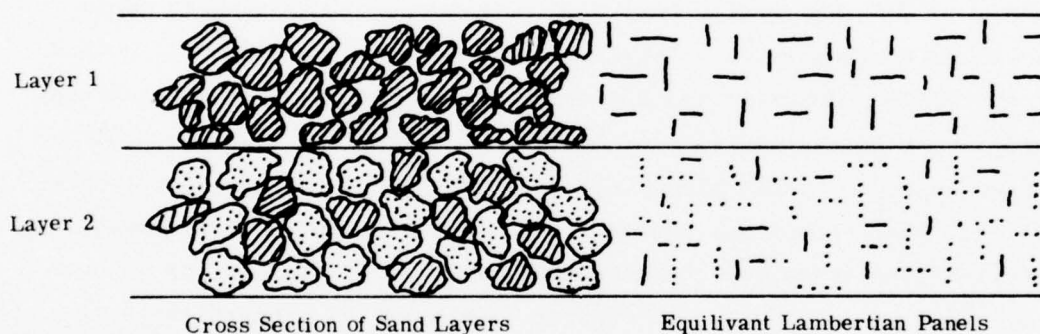
Because of the homomorphic relationship of radiative interactions with sand and vegetative canopies, the reflectance model previously developed for vegetation is applied to sand with the appropriate component properties for sand minerals substituted for vegetative canopies.

### 3.2.3 OPTICAL PROPERTIES OF SAND COMPONENTS

The cross section view of a hypothetical sand layer containing two kinds of mineral is shown in Figure 1. The irregular shapes of the sand grains result in some more or less random, loose packing with many voids. These grains are to be replaced by a number of equivalent Lambertian panels which will intercept approximately the same amount of radiant flux as do the actual grains. The spectral reflectance and transmittance of the panels are to be the same as the spectral reflectance and transmittance of the grains. Since these spectral properties may change with grain size or state of division, some means of calculating the appropriate spectral properties is required.

An auxiliary reflectance and transmittance model for mineral thin sections was developed in order to relate the inherent spectral properties which are characteristic of a mineral to the properties of that mineral in any state of division. Three characteristic bulk properties were taken to be sufficient for this purpose -- the spectral absorption coefficient,  $a$ , the forward scattering fraction,  $FS$ , and the scattering coefficient,  $s$ .

Radiation which penetrates a mineral may be absorbed and converted into heat energy depending upon the chemical composition of the mineral. A mineral which is internally homogeneous without inclusions and cracks will transmit radiation passing through it in accordance with the relation,



Layer 1 is shown as consisting of grains of only one kind of mineral.  
 Layer 2 is shown to consist of a mixture of two kinds of minerals.  
 The equivalent Lambertian scattering panels are illustrated on the right.

FIGURE 1. CROSS SECTION OF SAND LAYERS

$$E(x) = E_0 e^{-ax}, \quad (1)$$

where  $E(x)$  is the irradiance on a plane at depth  $x$  in the mineral,  
 $E_0$  is the irradiance on a plane inside the first surface,  
 $a$  is the spectral absorption coefficient.

The spectral absorption coefficient will be a function of the wavelength of the penetrating radiation and will depend upon the chemical composition of the mineral. The spectral absorption coefficient is largely responsible for the spectral variations in mineral reflectance and transmittance.

The formation of minerals is a complex natural process so that minerals may not be optically homogeneous. Foreign materials are often formed in the interior of the mineral. Such features as fractures, gas bubbles, small crystals of associated minerals, and grain boundaries of anisotropic crystals create inhomogeneities within mineral bodies. These inhomogeneities reflect or scatter and deviate penetrating radiation from rectilinear propagation. A collimated beam of radiation which propagates rectilinearly through the body of a mineral will be diminished due to such scattering by the relation,

$$E(x) = E_0 e^{-sx}, \quad (2)$$

where  $E(x)$  is the irradiance of rectilinear flux on a plane at depth  $x$ ,  
 $E_0$  is the irradiance of rectilinear flux at the first surface,  
 $s$  is the scattering coefficient.

The radiation which is scattered will tend to propagate either deeper into the mineral - forward scatter - and contribute to transmittance or reverse direction and propagate back out of the mineral - back scatter - and contribute to reflectance of the mineral. The

fraction of scattered radiation which continues deeper into the mineral is the forward scattering fraction, FS. The fraction of scattered radiation which reverses is then (1-FS). The scattering coefficient and the forward scattering fraction can be spectrally dependent but should not be the primary determinant of the spectral quality of a mineral.

These three optical properties of a mineral,  $a$ ,  $s$ , and FS, are assumed to be independent of the thickness of the mineral. That is, the inhomogeneous structure and chemical composition of a mineral thin section is assumed to be evenly distributed so that  $a$ ,  $s$ , and FS, are inherent properties characteristic of the kind of mineral and not the size of the mineral sample.

The auxiliary reflectance and transmittance model for mineral thin sections makes use of these three properties and the index of refraction of the mineral to yield the thin section transmittance and reflectance for any mineral thickness. The value of  $a$ ,  $s$ , and FS, for each wavelength must be determined experimentally. However, these properties cannot be determined by direct experiment. Instead, a spectrometer is used to measure the transmittance and reflectance of mineral thin sections having various thicknesses. Since  $a$ ,  $s$ , and FS are presumably thickness invariant, the value of  $a$ ,  $s$ , and FS may be determined by finding the value of  $a$ ,  $s$ , and FS which, when used in calculating the transmittances and reflectances of thin sections having these various thicknesses, yield matching values for the reflectances and transmittances found experimentally. A computer iteration technique was used for this purpose.

Then spectral values of  $a$ ,  $s$ , and FS for some of the common sand minerals have been tabulated. For certain opaque minerals, such as hematite and limonite, the values of  $a$ ,  $s$ , and FS could not be determined. The transmittance and reflectance of these minerals are independent of grain thickness for all thicknesses that are likely to be found in sands. The reflectance and transmittance of pure, unstained

clear quartz is due almost entirely to surface effects which are also independent of grain thickness.

The optical properties of sand components are determined and are introduced into the sand reflectance model. The spectral transmittance and reflectance of the equivalent Lambertian panels for each mineral are determined using the auxiliary reflectance and transmittance model for mineral thin sections where the thickness of thin section is the mean grain thickness for each mineral. The mean cross section of grains of each mineral type is multiplied by the corresponding number of such grains per unit volume for a given beach sample and represents the scattering effect of the equivalent Lambertian panels.

#### 3.2.4 MODEL SOFTWARE DESCRIPTION

Figure 2 indicates the flow of information beginning with the raw experimental CARY transmittance ( $\tau$ ) and reflectance ( $\rho$ ) data and ending with the predicted reflectance spectrum for sand. As indicated in section 2.2.3 the needed input into the SANDREF and AQUASANDREF model are transmittance,  $\tau$ , and reflectance,  $\rho$ , values for the individual minerals in a particular sand configuration. These  $\tau$  and  $\rho$  values must be calculated for each particle size. Experimentally,  $\tau$  and  $\rho$  spectra were determined for each mineral at given thicknesses. The minerals selected are shown in Table 1. Some minerals which were opaque exhibited a negligible amount of transmittance. Iron stains were treated as separate minerals and experimental  $\tau$  and  $\rho$  spectra were determined for them. These files are represented in the first row of Figure 2.

In order to predict  $\tau$  and  $\rho$ 's for any particle size, properties independent of size can be determined. These properties previously discussed on the forward scattering (FS), scattering coefficient ( $s$ ) and the spectral absorption coefficient ( $a$ ). The program ABSCAT (see Figure 2) calculates these coefficients for a given mineral using the experimental  $\tau$ 's and  $\rho$ 's, the experimental thicknesses and the parameters

TABLE 1  
COMMON BEACH FORMING MINERALS

Quartz  
Poly-crystalline Quartz  
Milky Quartz  
Orthoclase  
Plagioclase  
Kaolinite  
Hematite  
Chlorite  
Olivene  
Muscovite  
Hornblende  
Pyroxene  
Garnet  
Magnetite  
Ilmenite  
Carbonate

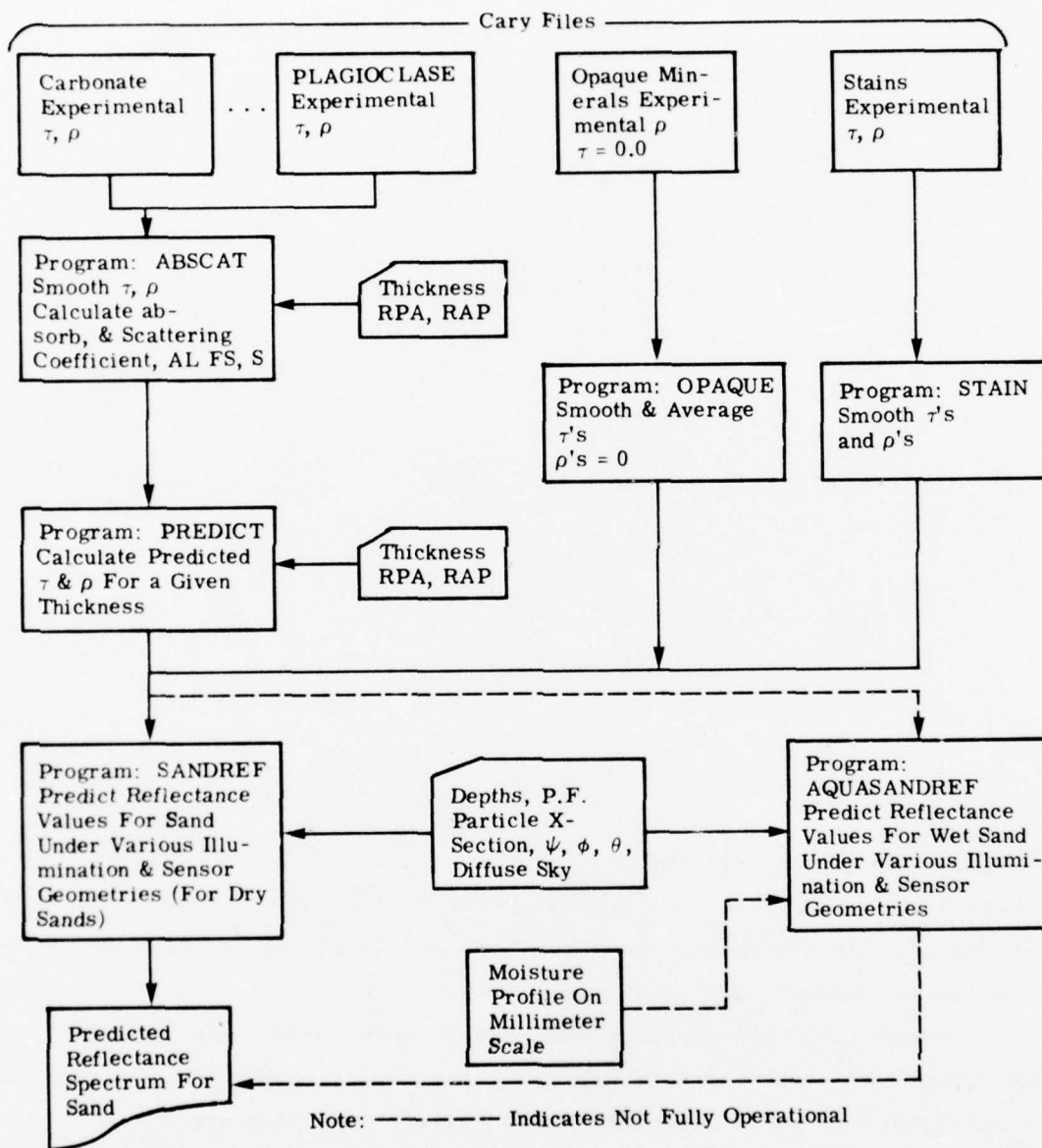


FIGURE 2. MODEL FLOW

RPA and RAP (related to the index of refraction). The experimental data is first smoothed to eliminate anomalies due to the experimental procedure. The equation for this smoothing is as follows for  $\lambda_1$  to  $\lambda_n$ .

$$\begin{aligned} \tau'(\lambda_1) &= \tau(\lambda_1) \\ \tau'(\lambda_2) &= \frac{\tau(\lambda_1)}{4} + \frac{\tau(\lambda_2)}{2} + \frac{\tau(\lambda_3)}{4} \\ &\vdots \\ \tau'(\lambda_I) &= \frac{\tau(\lambda_{I-1})}{4} + \frac{\tau(\lambda_I)}{2} + \frac{\tau(\lambda_{I+1})}{4} \quad (3) \\ &\vdots \\ \tau'(\lambda_n) &= \tau(\lambda_n) \end{aligned}$$

for all  $\lambda_I = \lambda_2$  to  $\lambda_{n-1}$ .

The next program is PREDICT. This program uses the scattering and absorption coefficients and the parameters RPA and RAP to predict  $\tau$ 's and  $\rho$ 's for a given thickness. These predicted values are now ready to be used to model the sand.

Theoretically all minerals can be processed through the ABSCAT and PREDICT programs. But as mentioned previously some minerals cannot be modelled this way. Opaque minerals fail this model because the transmittances are nearly zero. The program OPAQUE smooths the experimental reflectances and averages these  $\rho$ 's for all thicknesses used. The transmittances are set to zero for the whole spectrum. An important assumption made is that these average reflectances are the same for all sizes of particles.

Stains (e.g., iron stain) are also treated as minerals. The stains cannot be processed in the ABSCAT and PREDICT programs because these programs require at least two experimental thicknesses to make a prediction. The experimental  $\tau$ 's and  $\rho$ 's were only determined at one thickness for iron stain. Thus the program STAIN simply smooths the experimental values. The assumption to be kept in mind is that these smoothed values hold for all thicknesses of stain.

The program SNADREF computes the reflectance of mixtures of minerals. The inputs to this program consist of the predicted  $\tau$ 's and  $\rho$ 's for the minerals constituting the sand, the amount of iron stain, the depth of the sand, the reflectance of an infinite depth background underneath the sand, the particle cross sections and packing factors for the various minerals, the angle of illumination from a point source illuminator (or optional Lambertian source) and the angular position of the sensor.

The output of SANDREF is a predicted reflectance spectra of the sand for various configurations of illuminator position ( $\theta$ ) and sensor position ( $\phi, \psi$ ). The SANDREF program was derived from a program which predicted reflectances for a two layered vegetation canopy with a background. Thus the sand can have two layers with different densities and grain sizes in each layer. A background material for the sand can also be specified. These properties of SANDREF allow great flexibility for modeling various configurations such as thin sands, sand after a storm with a layer of organic matter or stones on top, etc.

AQUASANDREF is also indicated on Figure 1. Although not fully operational at the present time this model is very similar to SANDREF and essentially requires the same inputs with the addition of moisture information on a millimeter scale. Appendix A of this report includes a description of all the ONR developed beach environment computer programs. Included with the description of the program are the experimental derived  $\alpha$ ,  $s$ , and  $FS$  for one of the common beach forming minerals used in this

study. The  $\alpha$ ,  $s$ , and FS values of these minerals are the first reported values in the 0.4-2.5  $\mu\text{m}$  range.

### 3.2.5 PRELIMINARY MODELING RESULTS

Two beaches were selected for preliminary evaluation of the SANDREF model, one carbonate and the other principally quartz. The carbonate sample was collected from the ocean side at Marathon Key, Florida. The sample is comprised of rounded and plate carbonate shell fragments, calcareous algae flakes, and a trace of black carbonate debris. Figure 3 shows a reflectance curve in the 0.4-2.5  $\mu\text{m}$  region of a sample of the beach. The sample was measured using the ERIM Cary 14 spectrophotometer. The curve of the actual measured reflectance appears as a solid line. Superimposed on Figure 3 appears the generated SANDREF reflectance of the carbonate beach. This curve is dotted. The results are very encouraging, for although the absolute value of the curves differ, the overall shape and absorption bands seem to correspond remarkably well. After comparing the generated carbonate reflectance to the CARY reflectance of the actual sample, the original beach samples reflectance in the visible region was measured by use of a photo-detector and calibrated Lambertian reflectance panel. The results indicate that the Cary value for the carbonate beach sample is high. An examination of the Cary data is currently underway.

A quartz beach was also used in the preliminary evaluations of SANDREF. The quartz beach selected was from Mexico beach, Florida (previously described [1]). Original mineralogy information on this beach indicated it was 100% quartz with no iron stain. When SANDREF was run under this assumption, the results proved unsatisfactory. Consequently, the Mexico beach sample was reexamined and it was found that slight iron staining, black organic matter (1%), and some carbonate material existed in the sample. SANDREF was again run, this time with 95.5% quartz, 2.5% carbonate 1% illmenite (our substitute for black

organic matter), and 1% iron stain. The results are shown in Figure 4. As in Figure 3 the solid line curve represents the Cary obtained reflectance of the actual sample while the dotted line is the generated SANDREF reflectance. These results appear in close agreement.

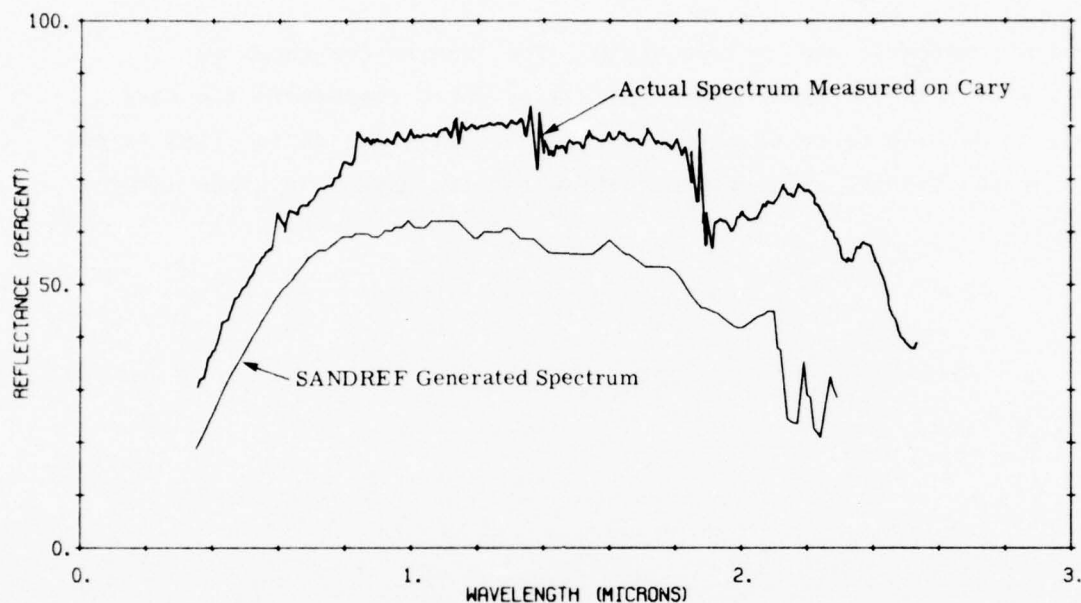


FIGURE 3. COMPARISON OF MEASURED CARBONATE REFLECTANCE WITH SANDREF MODEL RESULTS.

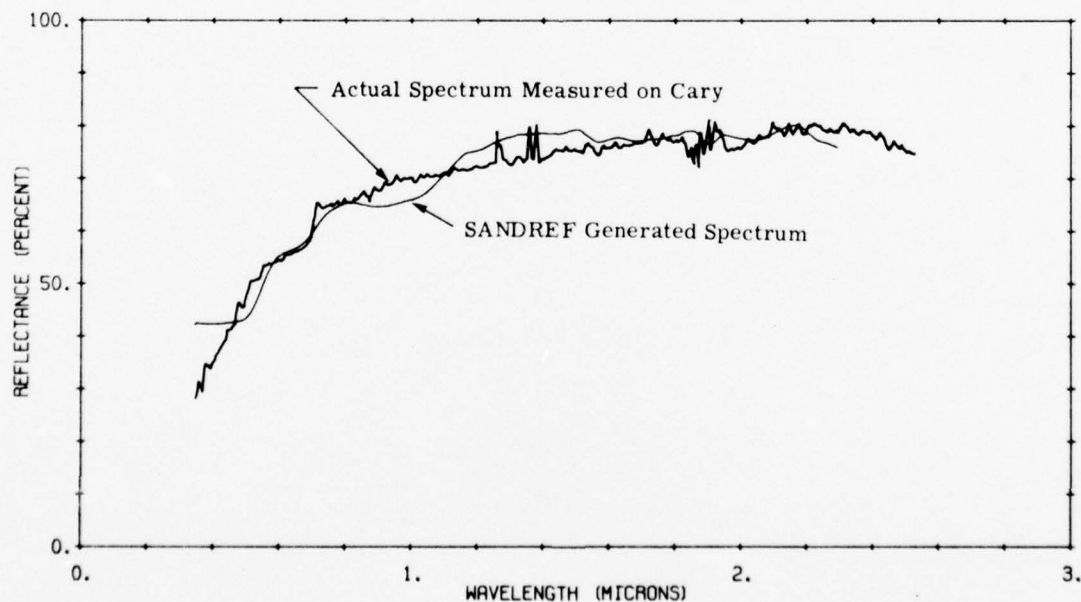


FIGURE 4. COMPARISON OF MEASURED QUARTZ REFLECTANCE WITH SANDREF MODEL RESULTS.

### 3.3 ASSESSMENT OF RADIATION PENETRATION IN BEACH SANDS

#### 3.3.1 RATIONALE

The depth to which radiation penetrates beach samples (skin depth), and depth below which changes in beach parameters do not contribute to the radiance viewed by the sensor, are of utmost importance understanding the limitations of remote sensing techniques for beach reconnaissance. First, we must understand which portion of the beach we are sensing with the passive techniques. If we are sensing properties of a layer of beach less extensive than that needed for trafficability analyses, approaches to correlate the remotely sensed information with the trafficability model requirements must be devised. Second, we wish to be sure that the 2-3 cm thicknesses of sand that were measured in the Cary 14 spectrophotometer were optically thick, so that the effect of the Cary 14 sample holder reflectance is minimal. Alternatively, if the samples were not optically thick, we would have to derive appropriate corrections for the library spectral data previously measured.

#### 3.3.2 DESCRIPTION OF SKIN DEPTH MEASUREMENTS

The purpose of the skin depth experiment was to obtain some estimates of the maximum depth which 0.6-1.1  $\mu\text{m}$  radiation would penetrate a sand layer and be back-scattered sufficiently to affect the radiance seen by a passive sensor, and to verify estimates of this depth calculated by the G. Suits model. Results of the G. Suits SANDREF model indicate that the skin depth for quartz beaches should not exceed 1 cm. These calculations also indicate that coarser grained sands and sands with increasing moisture content (above 15% by volume) have larger skin depths. To confirm these theoretical calculations, it was decided to obtain empirical measurements.

An experiment was designed to mimic both the CARY 14 optical configuration and potential remote sensing geometry, as shown in Figure 5.

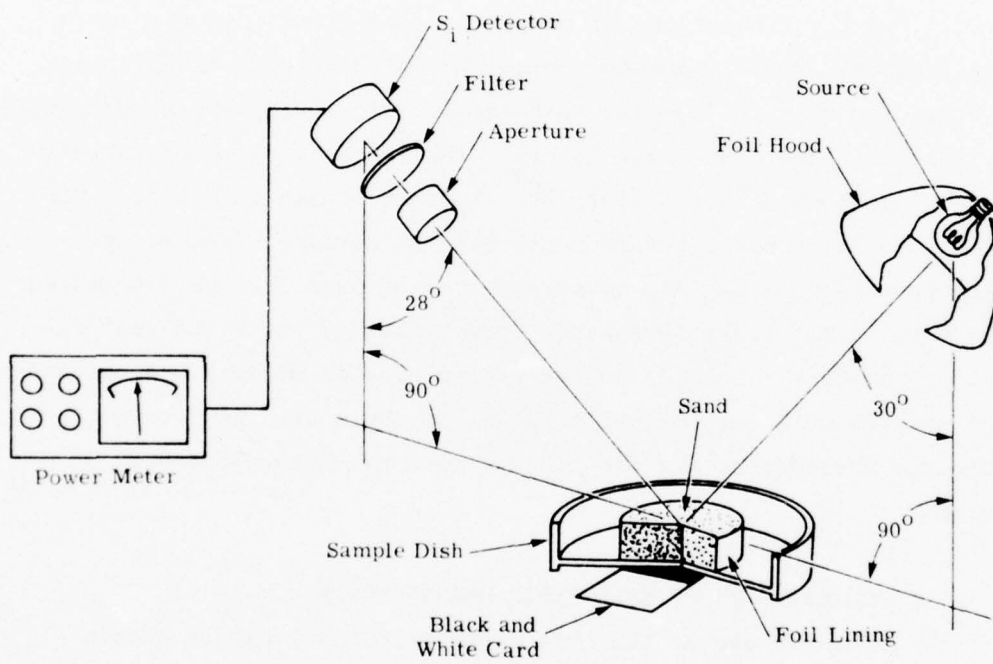


FIGURE 5. SKIN DEPTH MEASURING APPARATUS.

The inside of the sample dish was lined with aluminum foil to contain all incident light within the sample and avoid losses through the side of the dish. The source used was a GE 1323 tungsten filament densitometer bulb fitted with an aluminum foil cone. The sensor we used was a Coherent Radiation Model 212 power meter coupled with a silicon detector having a 1.1  $\mu\text{m}$  cut-off.

The detector was fitted with a .643  $\mu\text{m}$  (deep-red) C2-5B Corning filter. This reduced the spectral band of operation to approximately .643-1.1  $\mu\text{m}$ . A flat black cylinder was fitted to the detector head to provide greater directionality. After each sand sample was placed in the dish, a flat black cardboard ring was placed on top of the sand to minimize extraneous light reflection.

The actual measurement of skin depth was achieved by sliding a black card, then a white card under a petri dish filled with various thicknesses of sand. If fluxuations of greater than 1% of the total incident power were noted on the power meter it was concluded that light was penetrating the sand layer. More sand was then added to the petri dish and the test was repeated. When the power fluxuation was reduced to 1% of the incident power, the thickness of sand was recorded.

Five sand samples with various percentage of water by volume were tested. Samples were selected which varied greatly in both grain size and mineralogical composition so that the results could be generalized to all the sand types included in the fifty sample spectral reflectance data base.

### 3.3.3 RESULTS OF SKIN DEPTH MEASUREMENTS

Table 2 summarizes the skin depth measurements. The depths are given in millimeters as a function of percent moisture by volume. The sample numbers are the same as those in the previous interim report [1].

TABLE 2

RESULTS OF EMPIRICAL SKIN DEPTH MEASUREMENTS

SAMPLE NUMBER	SATURATED PERCENT MOISTURE BY VOLUME	Skin Depth In mm For Percent Water Content by Volume Shown						
		0%	5%	10%	15%	20%	25%	30% SATURATED
KAL	45.47	7	8	8	7.5	8	8	8-9 7-8
MX2	51.36	2	4	5	5	5	6	6 7
HA1	51.09	2.5	2.5	-	3	3	3	3 3
CA2	44.14	4	4	4	5	5	5-6	6 7
BD1	45.75	3.5	7	6	7	6	6	7 3.5

The results are in complete agreement with Suit's theoretical calculations using the modified SANDREF Model. The measurements show no significant penetration beyond 8 mm for all the sand samples whether wet or dry.

Skin depth increases with water content as predicted by Suits. The coarser sand samples KA1 (2.67 mm mean grain size), CA1 (.81 mm mean grain size) and BD1 (.71 mm mean grain size) have larger skin depths than the fine grain samples MX2 (.21 mm mean grain size) and HA1 (.32 mm mean grain size), again in agreement with the theory. The empirical measurements also indicate skin depth decreases with increasing percentage of opaque minerals and of iron stain.

#### 3.4 PLANS FOR FUTURE BEACH ENVIRONMENT TASK WORK

As discussed previously, the collection and reduction of the mineral, moisture, and skin depth data was quite rigorous and consumed a large fraction of the effort allotted to this task. The actual operation and verification of the SANDREF and AQUASANDREF were not begun until the final quarter of the current year's effort.

For next year, the model verification begun this year will be more vigorously pursued. The verification program will be completed by calculating the reflectances of some of the multi-mineral sand samples using measured physical parameters as model inputs and comparing these with the CARY 14 measured values now stored in the data bank. Further software refinements of the SANDREF and AQUASANDREF models, to improve efficiency of operation, will be made. This effort will not be a large one, however.

During consistency analyses of the reflectance and transmittance values of the mineral samples obtained from the CARY 14 data, we noted that the reflectance and transmittance values totalled greater than 1. This is physically impossible and indicates discrepancies in the basic CARY 14 measurements. The problem was first noted in the measurements for iron stain and was subsequently found in other data. We feel that

the method used to measure the transmission of samples may be faulty -- some radiation incident on the sample may be leaking around the sample and impinging directly on the detector, causing transmission values to be too large. The cause of this effect will be more thoroughly explored next year, and the sample data corrected as appropriate.

The preliminary exercise of the SANDREF model this year indicates the importance of accurate mineralogical information about the sand samples. We feel that the accuracy required exceeds the accuracy of the data obtained on our fifty sample library. To provide an adequate model evaluation, we will repeat the mineralogical analysis for certain of the samples. Special care will be taken to account for trace and opaque minerals in predominantly quartz samples, for in these samples trace minerals appear to influence the spectral reflectance most dramatically.

Beach samples that will be used for the model verification will include the Atlantic, Delaware Bay, Oregon "heavy mineral beaches", Mexico Beach, Lake Michigan quartz-feldspar, Kaolinite, and Marathon Key carbonate samples.

Development will also continue on improved moisture and grain size algorithms. This will be accomplished using the proven SANDREF and AQUASANDREF models to calculate the reflectance of a number of beach samples of chosen composition and moisture profile. The composition of these beach samples will be selected in such a way as to verify the form of the moisture algorithm already postulated and to attempt to derive a more meaningful multispectral grain size estimation algorithm. The improved moisture algorithm will be generated in such a way as to be minimally sensitive to mineral composition and grain size. The limits of performance, accuracy, and skin depth as well as the optimum spectral channels to use will be determined for both the moisture and grain size algorithms.

## UNDERWATER FEATURES STUDY

The objective for this year's effort was two-fold: first, to develop a model for calculating radiances over shallow water as would be measured by an airborne sensor, and second, to use these calculations to evaluate and improve data processing techniques for mapping bottom features. We have chosen the modeling approach because it allows the simulation of any set of conditions and is thus equivalent to collecting an actual data set under ideal circumstances where all the relevant parameters are known. Furthermore, the model can be used to generate a data set with no noise, representing an ideal sensor, or with an arbitrary amount of noise, simulating the data collected by an actual sensor.

## 4.1 MODEL DEVELOPMENT

In order to calculate radiances occurring in the atmosphere above a body of water, a water radiance model was developed which is actually a combination of two radiative transfer approximations. In this model, the double-delta approximation developed by Turner [3] at ERIM is used to calculate solar irradiances and atmospheric effects, and an extension of the quasi-single-scattering approximation developed during last year's ONR contract [1] is used to calculate the water reflectance. The combined model includes the effects of atmospheric scattering of incident sunlight, reflection of light at the water surface, scattering and absorption of light by the water column, reflection at the bottom, and attenuation of the reflected light in the atmosphere.

A computer program was written in FORTRAN to implement this water/atmosphere model on the University of Michigan's Amdahl 470 computer. The program reads in four sets of input parameters, described below, and computes a set of radiances as a function of water depth. These

radiances, which may be viewed as a simulated remote sensing data set, are stored for later display and analysis.

The first set of input parameters read in are called scene parameters, because they describe the external conditions for which the simulation is to be made. These include the atmospheric visibility (or meteorological range), the scene elevation above sea level, the solar zenith angle, the atmospheric scattering functions, and the wavelengths at which the calculations are to be made. The program then calculates the optical thickness of the atmosphere, based on Elterman's [4] tables, and the direct and diffuse solar irradiance at the water surface.

The second set of input parameters describe the platform from which the radiances are observed, including the altitude of the platform and the view angles. After reading these parameters, the program calculates the sky radiance and the path radiance scattered into the sensor from the atmosphere.

The third set of input parameters are the water parameters: these are the diffuse attenuation coefficient of the water, the volume scattering function of the water, and the external water surface reflectivity. The latter quantity was included as an input parameter to allow for the effects of variable sea state, using the relationships established by Austin [5]. The surface-reflected radiance is then computed by multiplying this parameter by the sky radiance at the appropriate zenith angle.

The final set of parameters read include the bottom reflectivity and the range of water depths to be considered. These are read last to allow duplicate sets of calculation to be made for different bottom types. The water radiance is calculated using equations similar to those described in Appendix C of reference 1, with the following modifications. First, the diffuse, or irradiance, attenuation coefficient ( $K$ ) is used instead of the beam extinction coefficient ( $c$ ) to describe the water attenuation. The approximate relationship:

$$K = (1 - w_o F)c \quad (4)$$

established by Gordon et al [6] is assumed to exist between these coefficients,  $K$  being the more easily measurable and more widely reported quantity. Second, the contribution from internal reflection at the water surface is computed to all orders by assuming for this purpose that the upward radiance just below the water surface is isotropically distributed. This is a somewhat more accurate approximation than the first-order correction described in reference 1, and in particular yields the correct result in the limit of zero water depth [7], for a Lambertian bottom. Third, the water reflectance is computed separately for the direct (sun) and the diffuse (sky) components of the incident irradiance. The sky radiation is assumed to be isotropically distributed for this calculation.

Radiance calculations are made for each depth specified in the last set of parameters, and stored on an output device. These results are displayed and analyzed as described in the following section.

#### 4.2 PARAMETER SELECTION AND MODEL RESULTS

The utilization of the radiance model for simulation purposes is presently limited by the availability of basic water and bottom reflectance measurements. Jerlov [8] has tabulated spectral irradiance attenuation data for various water types, but no corresponding scattering data is presented. On the other hand, Petzold [9] has tabulated complete sets of parameters, including volume scattering functions, for water samples taken from a variety of locations, but only at one wavelength.

In order to calculate the volume scattering functions at other wavelengths, the total scattering function was considered to be made up of two components: a Rayleigh component, which varies inversely with the fourth power of the wavelength, and a particulate component, which was assumed to be independent of wavelength. The total Rayleigh

scattering coefficient at  $0.55 \mu\text{m}$  was taken to be  $0.002 \text{ m}^{-1}$  from Petzold's measurements on filtered sea water. The Rayleigh component at  $0.55 \mu\text{m}$  was subtracted from the total scattering function at this wavelength in order to obtain the particulate component. The Rayleigh component was then recalculated at each wavelength using the fourth-power law and added to the fixed particulate component to yield the total volume scattering function at each wavelength.

Jerlov's water types 1, 3, and 5 were selected as representative of the conditions typically encountered in remote sensing in the coastal zone. The corresponding scattering data sets were chosen by computing the irradiance attenuation coefficients from equation (1) for each of Petzold's water samples and selecting those which were most nearly equal to Jerlov's values at this wavelength. The data sets from Station 9 (AUTEC), Station 5 (HAOCE), and Station 2200 (NUC) were selected on this basis as corresponding most closely to water types 1, 3, and 5, respectively. The irradiance attenuation coefficients for these three water types are shown in Figure 6, while the corresponding volume scattering functions at  $0.53 \mu\text{m}$  are plotted in Figure 7.

In the absence of reliable spectral bottom reflectance measurements, the reflectance of Florida beach sand, Kansas soil (representing mud), and wheat leaves (representing green aquatic vegetation) were used to approximate the reflectance of actual bottom materials. The reflectances of these materials in the range of  $0.450$  to  $0.575 \mu\text{m}$  wavelength are shown in Figure 8.

Using these water and bottom parameters, radiances were calculated at a platform altitude of 1 km for clear sky conditions (23 km visibility) with a solar zenith angle of 20 degrees. Radiances were calculated at 1 meter depth intervals from 0 to 20 meters. A surface reflectance of 0.021 was used, which is valid for observation angles less than  $20^\circ$  and windspeeds less than 10 meters per second [5]. The atmospheric phase function for Deimendjian's [10] haze M (marine or coastal) size distribution was used for calculating atmospheric effects.

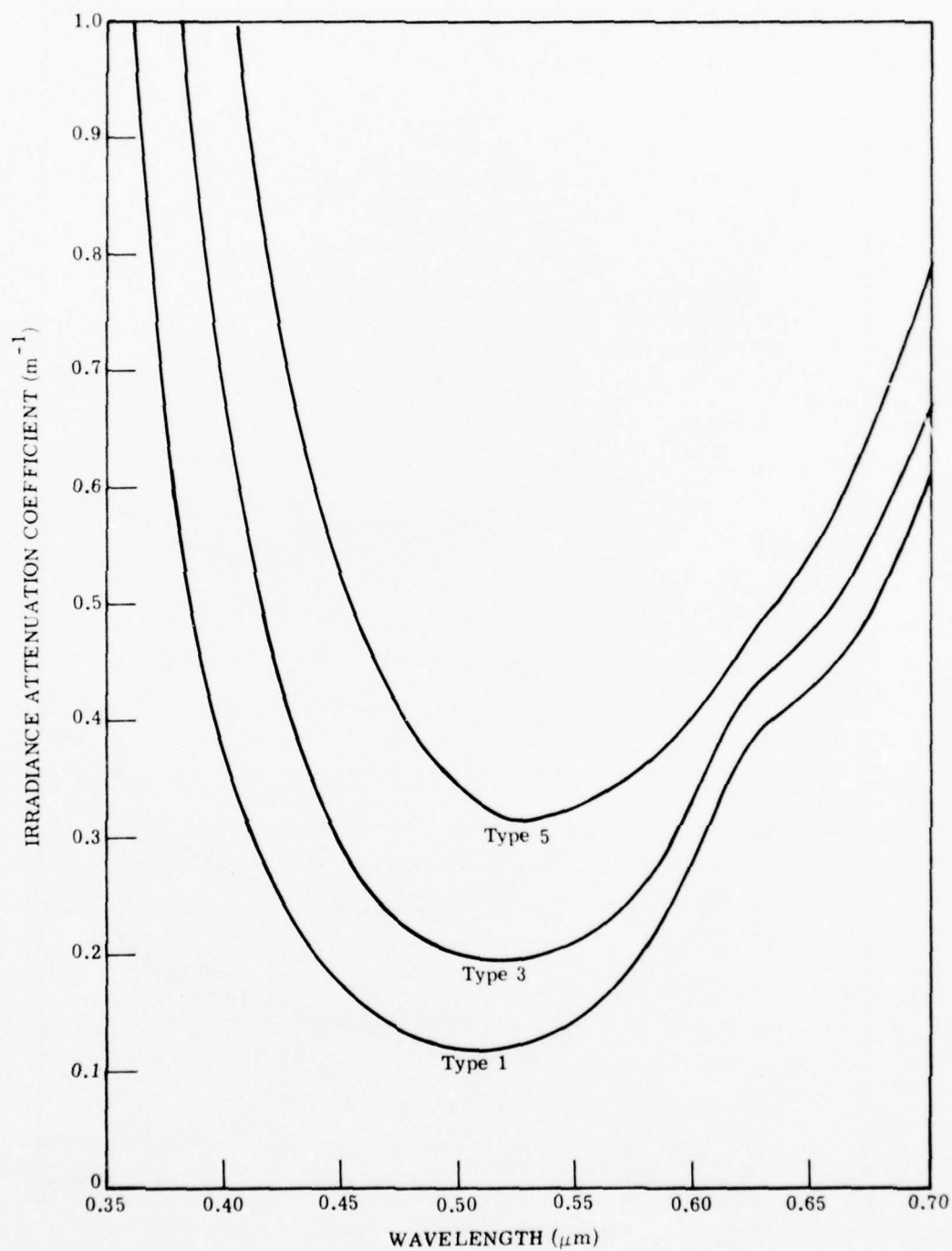


FIGURE 6. IRRADIANCE ATTENUATION COEFFICIENTS FOR JERLOV'S WATER TYPES 1, 3, and 5

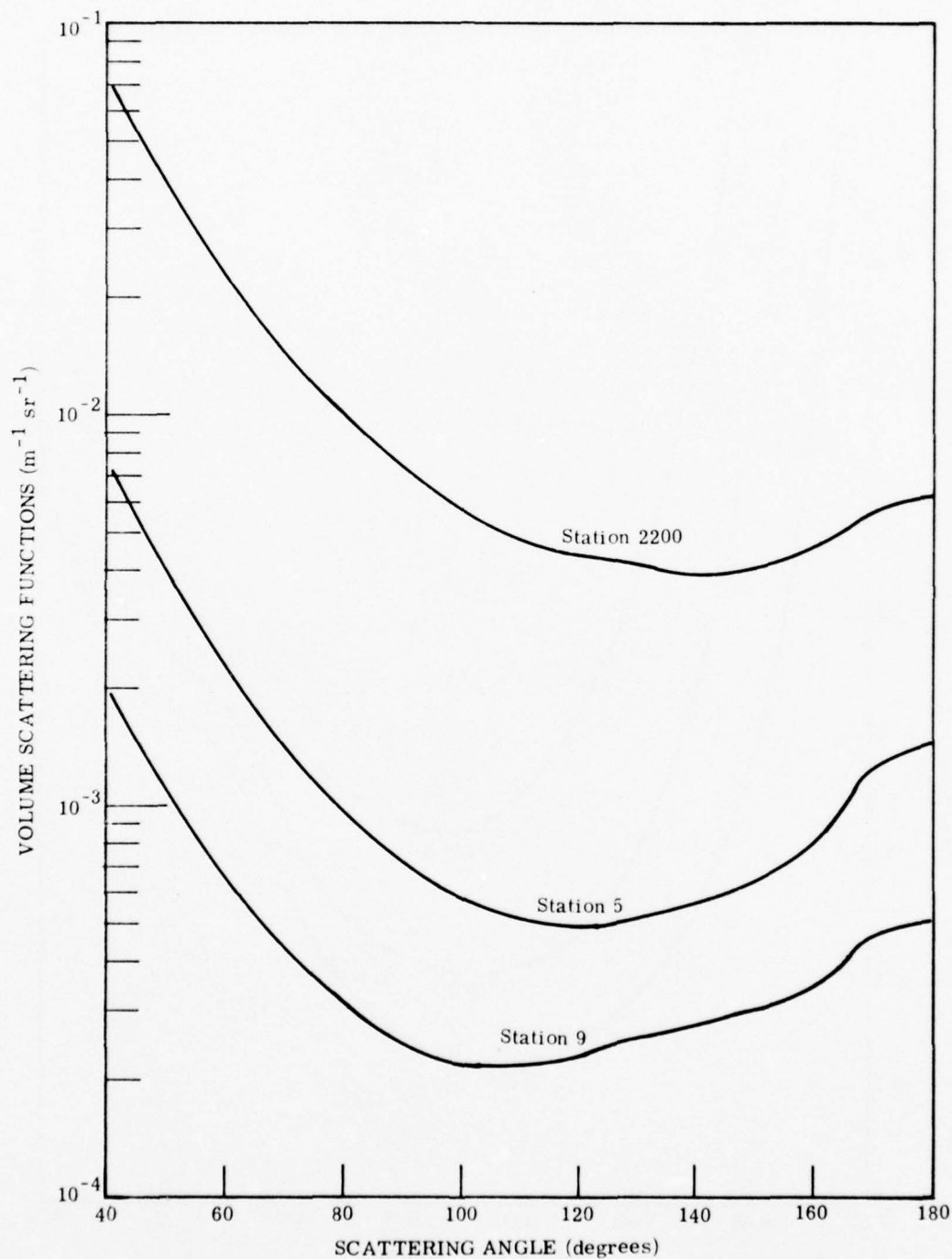


FIGURE 7. VOLUME SCATTERING FUNCTIONS VS. SCATTERING ANGLE FOR PETZOLD'S STATIONS 9, 5, AND 2200

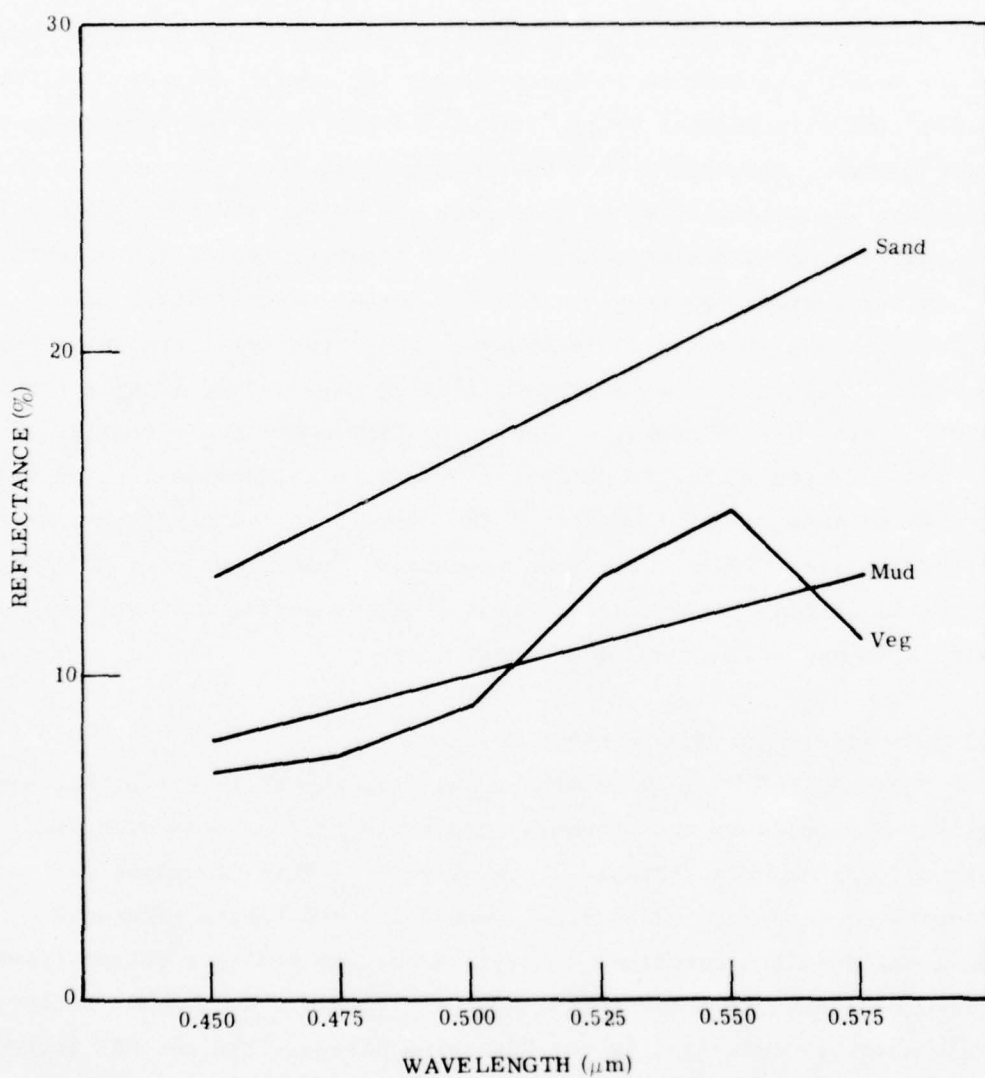


FIGURE 8. SPECTRAL REFLECTANCE OF SAND, MUD, AND GREEN VEGETATION

The resulting radiances may be displayed in several ways. One convenient form of display, which is useful for analysis of bottom features, is the two-channel plot shown in Figures 9 and 10. These figures show the "trajectory" of the signals as the depth varies from zero (upper right end) to infinity (lower left end). Figure 9 is for wavelengths with unequal water attenuation coefficients, showing curved trajectories. Figure 10 is for wavelengths with equal attenuation coefficients; the trajectories in this case are nearly straight, with only a slight curvature due to scattering and internal reflection effects.

Similar plots can be generated for actual scanner data, except that the actual data points are distributed around the ideal trajectory due to noise. Figure 11 shows a scatter plot of data values along a transect in St. Andrew Bay, Florida, collected by ERIM's M-7 Scanner [11]. The two trajectories indicated on this figure were calculated for the water parameters measured at the time of the overflight, with bottom reflectance ratios for sand (lower curve) and vegetation (upper curve). An abrupt change in bottom type occurs at about 2 meters depth, indicated by a shift from one trajectory to another.

#### 4.3 DESCRIPTION OF MRA TECHNIQUE

The modified ratio algorithm (MRA) uses the ratio of the bottom-reflected signals in two channels to discriminate between different bottom types under a variable depth of water. This technique is illustrated in Figure 12. Curves A and B in this figure represent the idealized "trajectories" of signals for two distinct bottom types. A line beginning at the point  $L_{1s}, L_{2s}$  with slope  $R$  is drawn between these curves: this line is the "decision boundary" in the MRA technique for discriminating between bottom types A and B. The values  $L_{1s}$  and  $L_{2s}$  are the "offsets" in channels 1 and 2, which are normally obtained by scanning over deep water. If a given set of observed radiances  $L_1$  and  $L_2$  fall above the decision boundary, the ratio value is greater than  $R$ , and

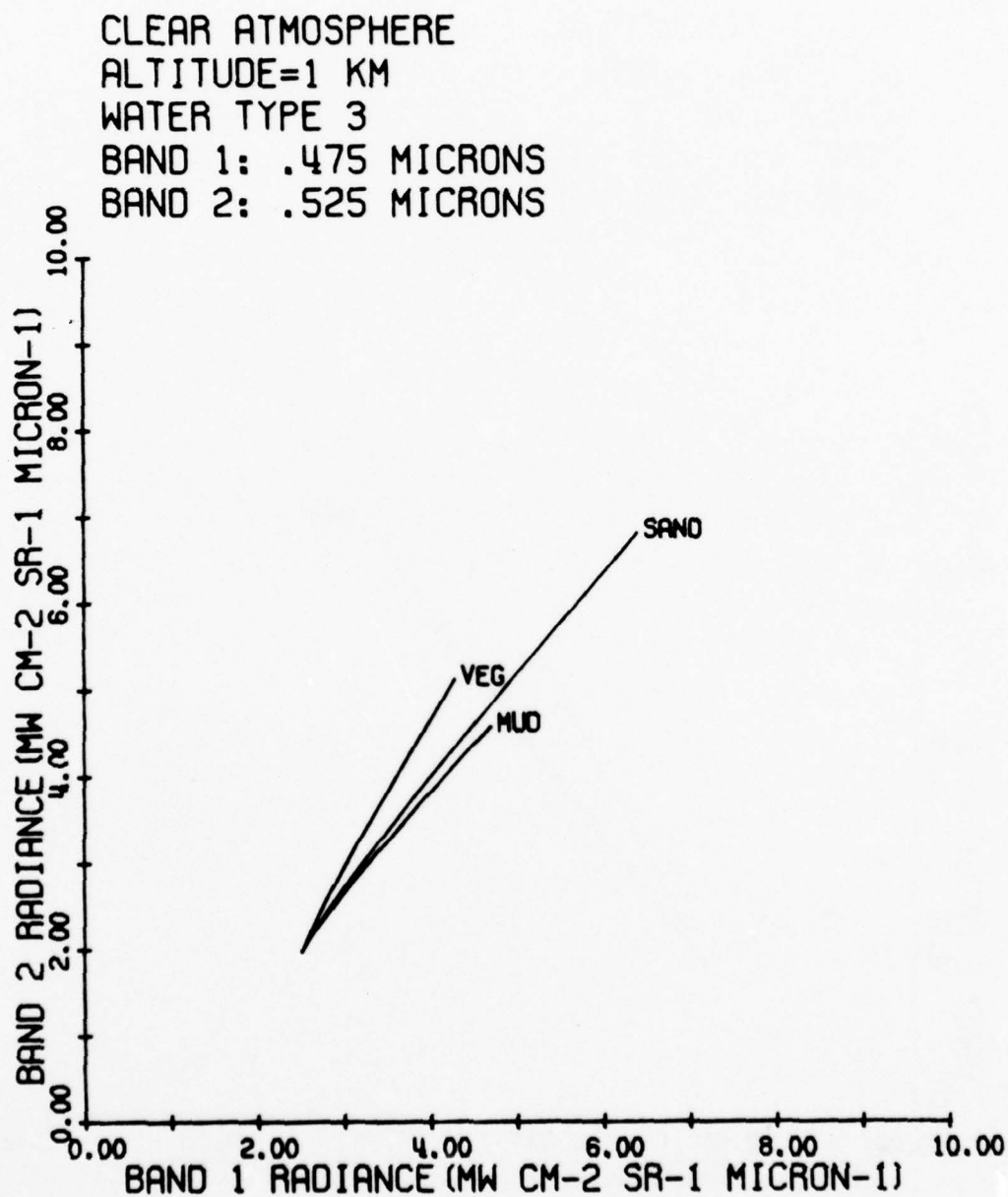


FIGURE 9. TWO-CHANNEL PLOTS OF RADIANCES OVER WATER TYPE 3

CLEAR ATMOSPHERE  
 ALTITUDE=1 KM  
 WATER TYPE 3  
 BAND 1: .485 MICRONS  
 BAND 2: .550 MICRONS

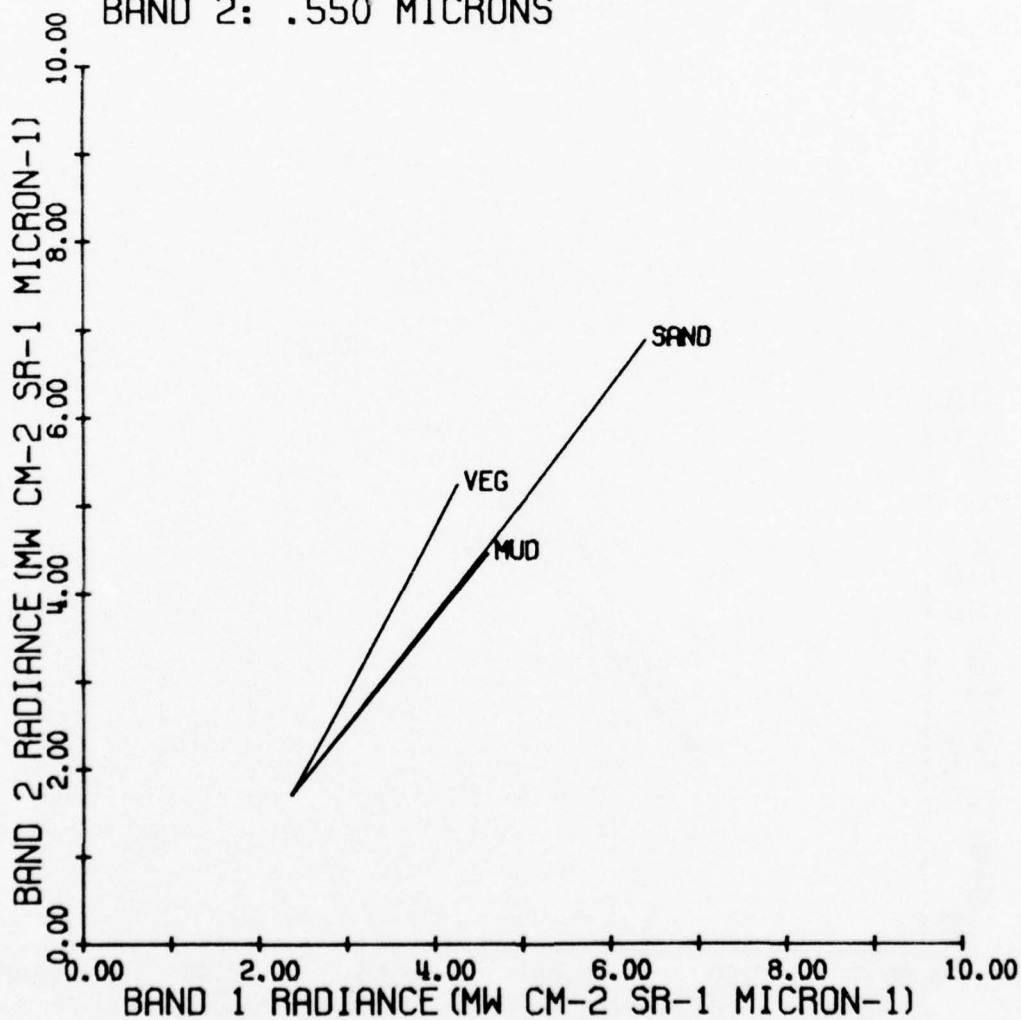


FIGURE 10. TWO-CHANNEL PLOT OF REFLECTANCE OVER WATER TYPE 3

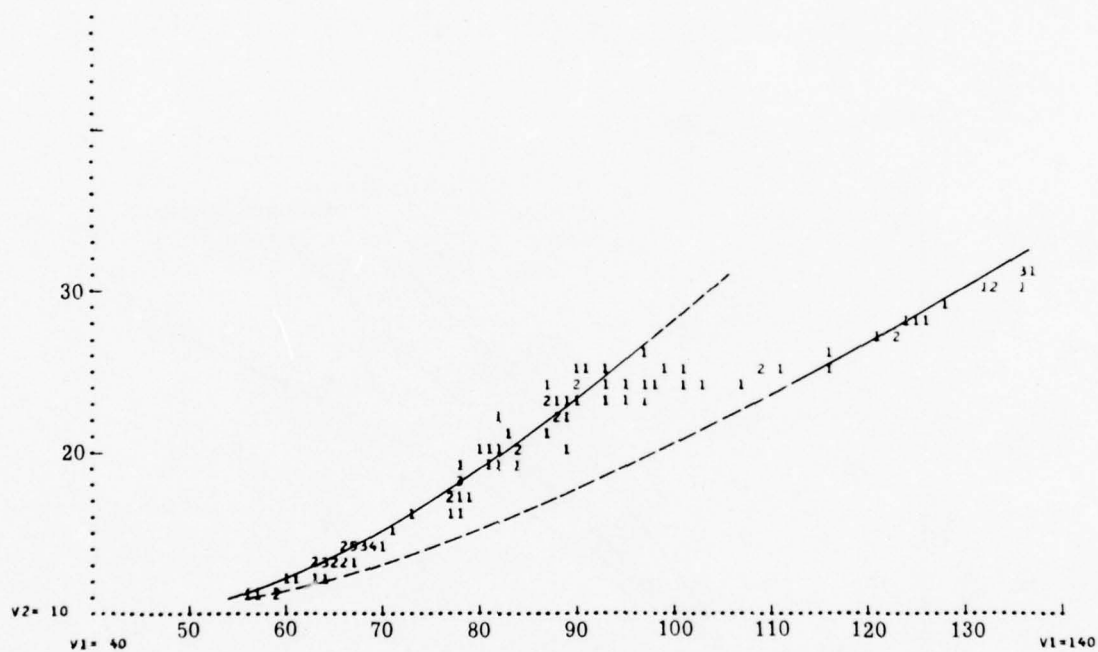
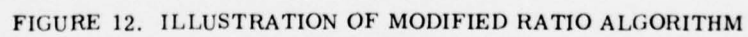


FIGURE 11. TWO-CHANNEL PLOT OF DATA VALUES FROM ST. ANDREWS BAY, FLORIDA.  
Curves indicate trajectories calculated for sand (lower curve) and vegetation (upper curve).



$$R' = \frac{L_2 - L_2 s}{L_1 - L_1 s} \quad (5)$$

the material is presumed to be bottom type A. All points below this line have a ratio value less than  $R$ , and are presumed to belong to bottom type B.

If the signal trajectories were straight lines, and if there was no noise in the signal, the MRA technique would allow a perfect discrimination between bottom types. The trajectories are nearly straight if the water attenuation coefficients in bands 1 and 2 are equal, but there is some curvature due to scattering and internal reflection effects. Further, system noise and variation of the surface-reflected signal due to waves cause the actual signals to be distributed around idealized trajectories rather than to fall exactly on them. For a given depth  $z'$ , the distribution of data points may be approximated by a Gaussian distribution

$$p(L_1, L_2) = \frac{1}{2\pi\sigma_1\sigma_2} \exp \left\{ -1/2 \left[ \left( \frac{L_1 - L_1'}{\sigma_1} \right)^2 + \left( \frac{L_2 - L_2'}{\sigma_2} \right)^2 \right] \right\} \quad (6)$$

where  $L_1'$  and  $L_2'$  are the radiances at the depth  $z'$  in the absence of noise, and  $\sigma_1$  and  $\sigma_2$  are the r.m.s. noise signals in bands 1 and 2. The ellipse drawn in Figure 12 represents one standard deviation of the radiance at  $z = z'$  due to noise. The equation of this ellipse is

$$\left( \frac{L_1 - L_1'}{\sigma_1} \right)^2 + \left( \frac{L_2 - L_2'}{\sigma_2} \right)^2 = 1 \quad (7)$$

and the probability that a given radiance measurement at depth  $z'$  will fall inside this ellipse is 39.3%. Suppose now that a similar ellipse is drawn tangent to the decision boundary (this ellipse is drawn as a dotted line in Figure 12). This ellipse is described by the equation

$$\left( \frac{L_1 - L_1'}{\sigma_1} \right)^2 + \left( \frac{L_2 - L_2'}{\sigma_2} \right)^2 = d^2 \quad (8)$$

where

$$d = \frac{\left( \frac{L_2 - L_{2s}}{\sigma_2} \right) - R \left( \frac{L_1 - L_{1s}}{\sigma_1} \right)}{\sqrt{\sigma_1^2 + R^2 \sigma_2^2}} \quad (9)$$

Using the probability distribution (6) it can be shown that the total probability that a given radiance measurement at depth  $z'$  over bottom type A will fall below the decision boundary is

$$P' = 1/2 \operatorname{erfc} \left( \frac{d}{\sqrt{2}} \right) \quad (10)$$

where  $\operatorname{erfc}$  is the complemented error function. This is equivalent to the probability of misclassification for the MRA with this decision boundary. In the case of three (or more) bottom materials, there are two (or more) decision boundaries. The probability of misclassification for a material having a decision boundary on both sides is then equal to the joint probability of a measurement falling beyond either decision boundary.

#### 4.4 EVALUATION OF MRA TECHNIQUE

A computer program was written to calculate the probabilities of misclassification for the MRA technique with the bottom materials and water types described in section 3.2. This program uses the radiance data computed by the radiance model program to simulate the performance of the MRA on an actual remote sensing data set. The r.m.s. noise signals are computed from the equation

$$\sigma = \sqrt{L_n L} \quad (11)$$

where  $L$  is the total radiance being measured and  $L_n$  is the noise-equivalent radiance of the sensor. For the ERIM M-7 scanner, the noise-equivalent radiance is approximately  $.001 \text{ mW cm}^{-2} \text{ sr}^{-1} \mu\text{m}^{-1}$  in the blue-green region of the spectrum.

The program is designed for interactive use so that various modes of operation can be selected. Among the user inputs are the wavelengths, offsets, and the water depth at which the algorithm is to be "trained". The ratio values for each bottom type are calculated at this depth, and the decision boundaries are chosen midway between each adjacent pair of ratio values. Having chosen the decision boundaries for each bottom material, the "distance"  $d$  between the decision boundary and the trajectory is calculated at each depth, from equation (9). The probability of misclassification is then calculated from equation (10) as a function of depth for each bottom type.

The results of one such set of calculations are shown in Figure 13. These results are for water type 3, with wavelengths selected to maximize the separability of green vegetation, subject to the constraint that the attenuation coefficients must be the same at both wavelengths. The results show that vegetation is indeed the most accurately classified bottom type, with a probability of misclassification less than 25 percent out to a depth of about 5 meters.

The relatively poorer performance over sand and mud is due to the similarity in the shape of their spectral reflectance curves. This can be seen in Figure 10, which shows that the signal trajectories for sand and mud are very close together for these wavelengths. This limitation of the MRA technique will be further discussed in the following section.

The performance illustrated in Figure 13 is obtained if the water quality is uniform throughout the scene. In actuality, water quality is likely to be non-uniform in the coastal environment because of wave action, runoff from the land, and biological activity nearshore. In the typical situation the water quality is similar to water type 1 in deep water, and to water type 3 or even water type 5 in shallow water (although water type 5 is usually more typical of inland waters). The effect of these changes in water quality is two-fold. First, since the offsets are usually obtained by scanning over deep water, these offsets will be incorrect if the water quality in deep water is different from that in shallow water. Second, since the optimum wavelengths and decision boundaries vary with water quality, an algorithm which has been optimized for one water type will perform less well in another water type.

The effects of such changes in water quality are illustrated in Figures 14 and 15. Figure 16 shows the MRA performance for vegetation in three situations. Curve A is for uniform (type 3) water quality throughout the scene (i.e., the same situation as in Figure 13. The offsets were obtained from water type 3 and the operating parameters (wavelengths and decision boundaries) were optimized for the same water type. Curve B shows the performance in water type 3 with offsets obtained from water type 1, but with the algorithm otherwise optimized for water type 3. Curve C shows the results of the same algorithm applied to water type 5: that is, the offsets were obtained from water type 1, the algorithm was "trained" in water type 3, and the performance was evaluated in water type 5. Figure 15 shows the average performance for the three bottom types in the same three situations.

The performance in shallow water is approximately as expected. The average probability of misclassification is the smallest for the optimized algorithm (curve A) out to about 7 meters depth. The

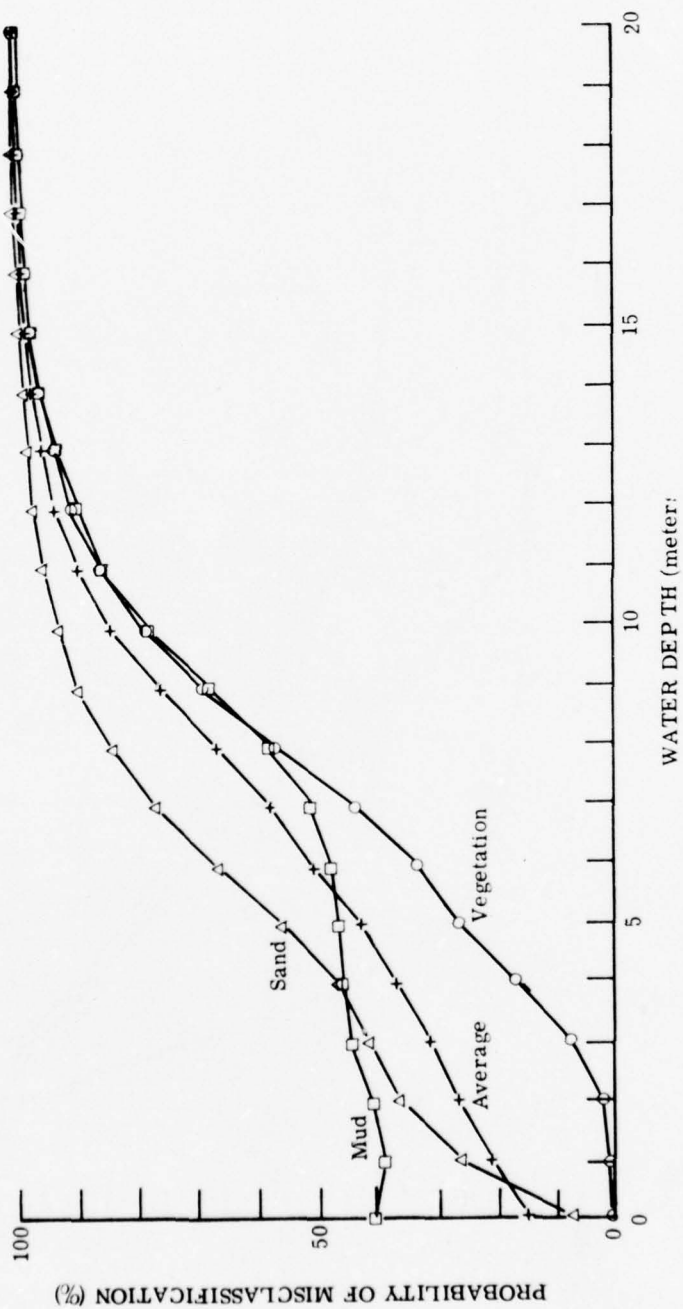


FIGURE 13. PROBABILITY OF MISCLASSIFICATION VS. DEPTH FOR WATER TYPE 3

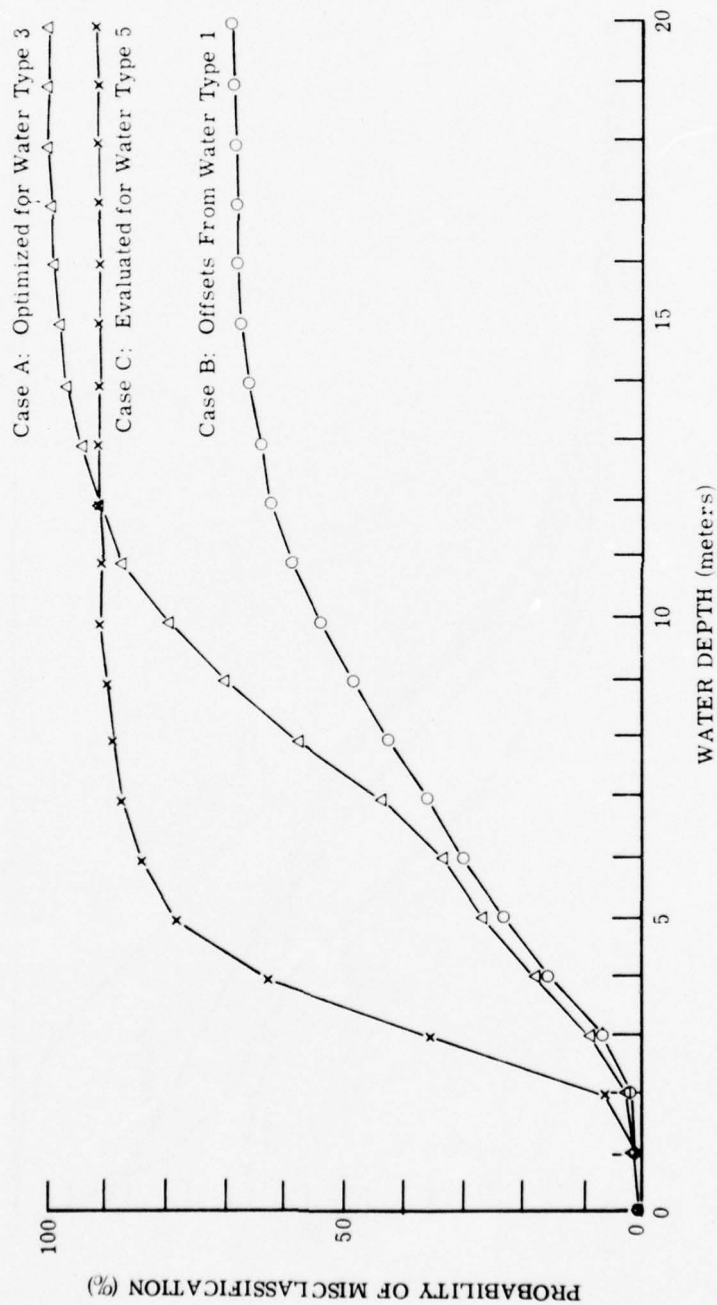


FIGURE 14. PROBABILITY OF MISCLASSIFICATION FOR VEGETATION VS. DEPTH IN THREE SITUATIONS

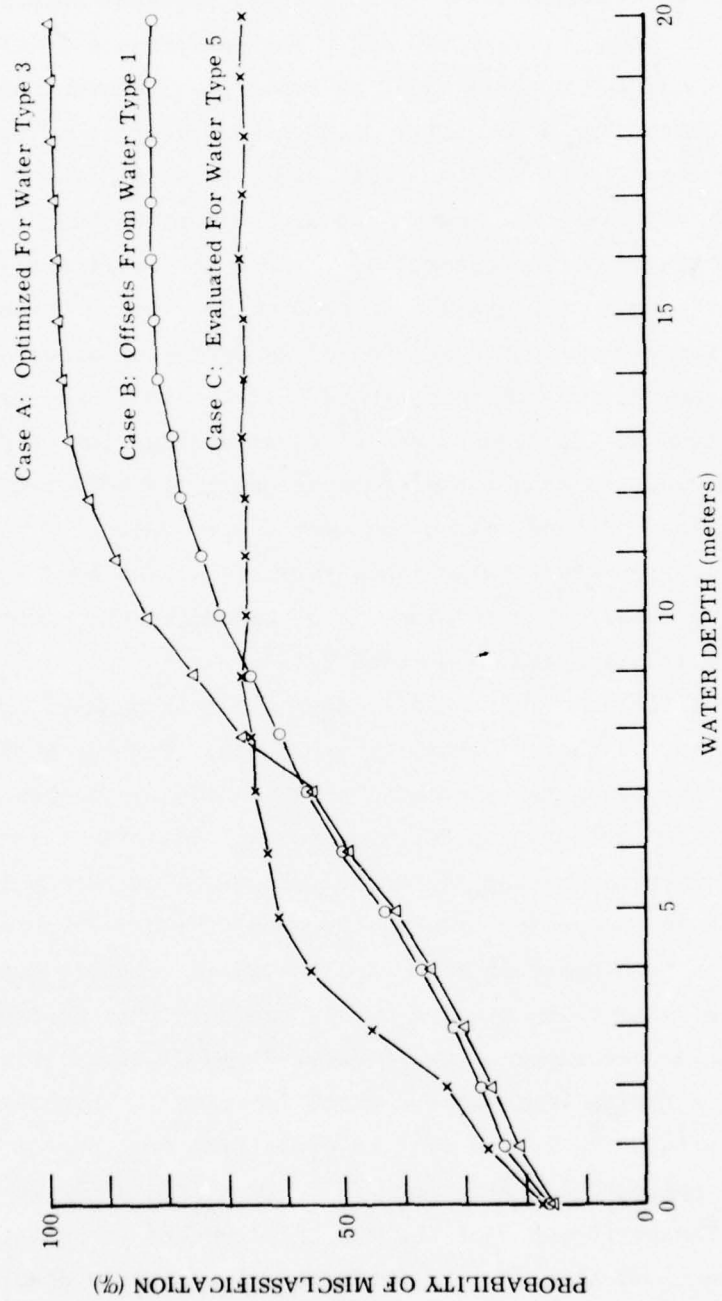


FIGURE 15. AVERAGE PROBABILITY OF MISCLASSIFICATION FOR THREE BOTTOM TYPES VS. DEPTH IN THREE SITUATIONS

performance in situation B is fortuitiously somewhat better for vegetation, but is worse for sand and mud. The performance in situation C is also worse than the optimum case, as expected. Somewhat surprisingly, however, the average probability of misclassification is relatively high (17%) even at zero depth. This suggests a fundamental limitation of the MRA: namely, that the bottom discrimination technique used in this algorithm is not an optimal one, since it incurs a relatively large error even in the absence of an overlying water column. There are two reasons even in the absence of an overlying water column. There are two reasons for this error. First, the choice of wavelengths is constrained by the requirement of equal attenuation coefficients, and the wavelengths cannot therefore be optimally selected for bottom discrimination. Second, since the method uses ratios of signals, bottom types with nearly equal reflectance ratios (such as sand and mud) are not well separated. The development of algorithms not subject to these limitations is discussed in section 3.5.

The performance of the MRA in deep water is perhaps counter-intuitive, but can be quite easily explained. For the optimized algorithm, the probability of misclassification approaches 100 percent for all bottom types as the depth approaches infinity. This is to be expected, since the bottom cannot be recognized correctly if it cannot be seen. When the proper offsets are used, the numerator and denominator of the ratio both approach zero, and the ratio value is dominated by noise: i.e., the value becomes purely random. When an improper offset is used in the denominator (as in cases B and C), the ratio value approaches a finite limit as the depth increases. Therefore, the probability that the bottom will be classified into one or more of the categories approaches a non-zero limit, even though the bottom cannot be seen. The performance of the MRA thus appears to be better for the non-optimum cases than for the optimized algorithm in deep water. In practice, probabilities of misclassification greater than 67 percent

(for a three category situation) are not of interest anyway, since this is the probability of misclassification for a purely random guess.

A summary of the MRA performance in the three water types is shown in Table 3. The number in the first column indicates the water type in which the evaluation was performed. The second column indicates the water type from which the offsets were taken, and the third column indicates the water type for which the algorithm was optimized. The last two columns contain the average probability of misclassification at zero depth, and the depth at which this probability is equal to 50 percent, respectively.

The first three entries in Table 3 represent fully optimized cases, in the sense that offsets were chosen from the same water type and wavelengths were chosen to equalize the attenuation coefficients. However, the wavelengths used for water type 1 were apparently more optimum than those for water type 3 from the point of view of bottom discrimination, since the probability of misclassification at zero depth is smaller for type 1 than for type 3. Similarly, the wavelengths for type 3 are better than those for type 5 for bottom discrimination. This explains why the MRA performance in water type 5 using the type 3 algorithm (the last case) is better than the performance using the "fully optimized" type 5 algorithm.

TABLE 3  
SUMMARY OF MRA PERFORMANCE

<u>WATER TYPE</u>	<u>OFFSETS</u>	<u>ALGORITHM</u>	<u>Pm(z=0)</u>	<u>z(Pm = 50%)</u>
1	1	1	13.2%	8.4 m
3	3	3	16.6%	6.0 m
5	5	5	26.7%	3.0 m
3	1	3	17.2%	6.0 m
5	1	3	17.2%	3.6 m

#### 4.5 FURTHER ALGORITHM DEVELOPMENT

The primary limitation of the MRA technique is its inability to separate bottom materials with equal or nearly equal values of the bottom reflectance ratio in the two operating channels. For such bottom types, the signal trajectories are coincident, or nearly coincident, as in Figure 10. This results in the relatively high probabilities of misclassification for sand and mud shown in Figure 13.

It is possible to select wavelength pairs with distinct signal trajectories for any set of bottom types, if the attenuation coefficients are not required to be equal. The trajectories in Figure 9, for example, are distinct even though the ratios of bottom reflectances are nearly the same for sand and mud. In this case, however, the trajectories cannot be separated by a linear decision boundary as in the MRA.

An alternative processing algorithm for this case is suggested by the approximately exponential relationship between signal levels and water depth. If the transformation:

$$V'_i = \ln (L_i - L_{is}) \quad (12)$$

is applied to the data and the results are plotted, the result is a set of nearly linear, parallel trajectories. Figure 16 shows such a plot for the same data set as plotted in Figure 9. The slope of these trajectories is given by the ratio of the attenuation coefficients in the two channels. Thus, a linear decision boundary can be drawn between each pair of trajectories to separate the bottom types. These decision boundaries are described by the equation

$$V'_1 - \frac{K_1}{K_2} V'_2 = C_j \quad (13)$$

where  $K_1$  and  $K_2$  are the attenuation coefficients in bands 1 and 2, and  $C_j$  is a different constant for each decision boundary.

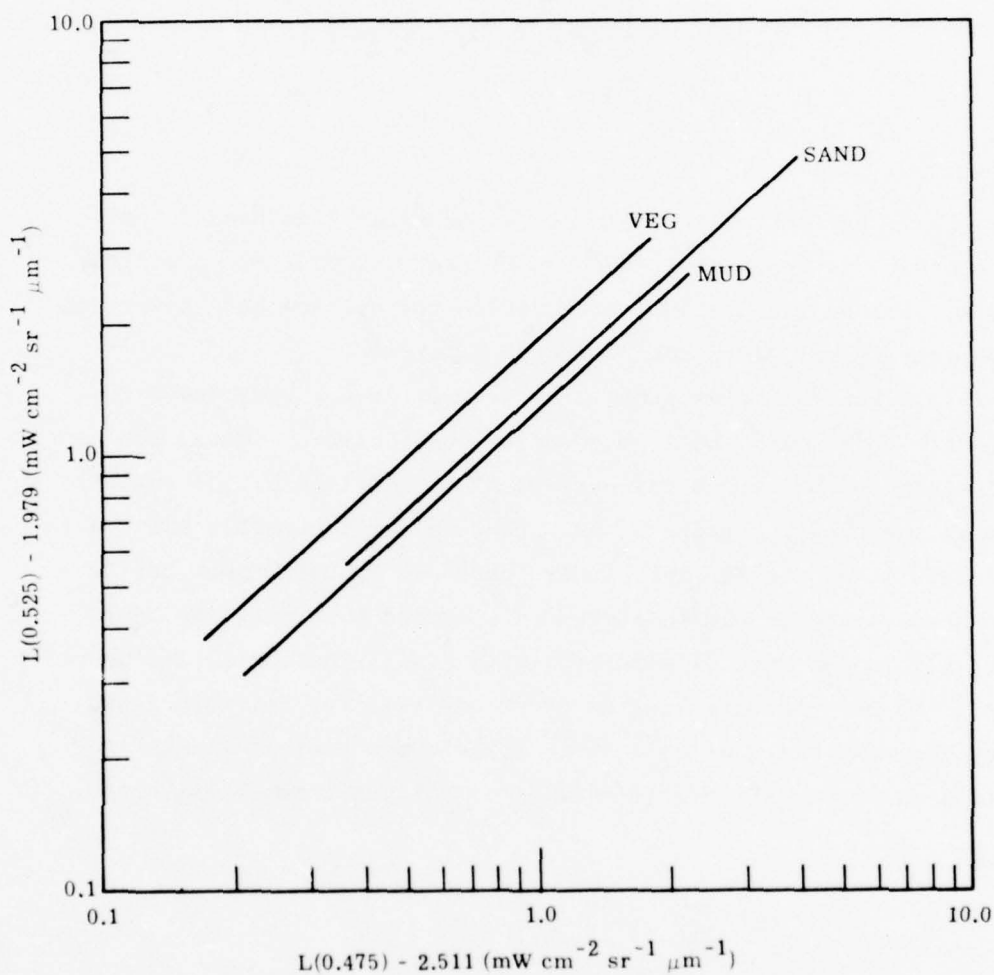


FIGURE 16. LOG-LOG PLOT OF BOTTOM-REFLECTED SIGNALS FOR WATER TYPE 3 AT 0.475 μm AND 0.525 μm

The "distance" between the trajectories of material A and material B are given approximately by the equation

$$S = \frac{K_2 \ln \left( \frac{r_{1A}}{r_{1B}} \right) - K_1 \ln \left( \frac{r_{2A}}{r_{2B}} \right)}{\sqrt{K_1^2 + K_2^2}} \quad (14)$$

where  $r_{1A}$  is the bottom reflectance for material A in band 1, etc. This equation is approximate because it neglects scattering effects. However, such an index allows a criterion for optimum band selection for separating any given set of bottom materials.

This algorithm holds promise because it is not restricted to wavelength pairs with equal attenuation coefficients. Thus, the wavelengths can be chosen for optimum discrimination of the bottom types in the scene. Further, the method is not inherently limited to two channels, as the MRA is. It is therefore expected that better performance could be obtained with this method than with the MRA, especially in the case of materials with similar bottom reflectance ratios. We hope to carry out an error analysis for this algorithm during the next year, as well as to include scattering effects in equation (13) and define a criterion for optimum channel selection.

APPENDIX A

DESCRIPTION OF ONR DEVELOPED BEACH ENVIRONMENT COMPUTER  
PROGRAMS INCLUDING SAMPLE OUTPUT

## A.1 DESCRIPTION OF PROGRAMS

### A.1.1 ABSCAT

The ABSCAT program calculates the absorption and scattering coefficients for a mineral when given the experimental transmittances and reflectances. The user invokes this program by typing

```
$RUN ABSCAT 1 = CONTROL FILE
```

where the control file contains a namelist input. An example of this control file follows:

```
&LIST  
RAP = .6, RPA = .03, PU = 5*1., PL = 5*0, DP = 5*.01, SIG = ,  
ITER = 20, NPAR = 5,  
& END
```

These parameters are defined as:

RAP - related to index of refraction  
RPA - related to index of refraction  
PU - parameter upper bounds (AL, FS, S)  
PL - parameter lower bounds (AL, FS, S)  
DP - parameter increment for curve fitting  
SIG - parameter error allowance  
ITER - number of iterations for Newton's method  
NPAR - number of parameter bounds used

The program will first prompt the user to declare mineral input and coefficient output files. The next prompt will be for the user to enter the sample number and thickness for the infinite thickness sample. If there is no infinite thickness, the user enters zero for the sample

number and the thickness of the first sample. The next prompt is for up to three transmittance sample numbers. The user will then be prompted for the corresponding reflectance numbers. The final prompt will be for the corresponding sample thicknesses. Note that if there was not any infinite thickness sample, the first sample thickness was already entered. Therefore, the remaining thicknesses should be entered.

#### A.1.2 PREDICT

The PREDICT program calculates predicted transmittance and reflectances given the scattering coefficients and the mineral thickness for which the prediction is to be made. The user invokes this program by typing

\$RUN PREDICT

The user will then be prompted to enter the output file and the input file which contains the scattering and absorption coefficients (output from ABSCAT). The next prompt will be for the mineral thickness at which to make the prediction and RAP and RPA.

#### A.1.3 OPAQUE

The OPAQUE program will take experimental reflectances for a mineral which were determined for different thicknesses and smooth this data using equation (3). The average reflectance over all thicknesses will be found. The program will then output a file compatible with the output of PREDICT that contains the smoothed and averaged reflectances and all transmittances set to zero. The user will be prompted for the input file, output file, and experimental thicknesses. Up to four thicknesses may be used. The user invokes this program by typing

\$RUN OPAQUE

#### A.1.4 STAIN

The program STAIN will take an input file containing one set of experimental transmittance and reflectance spectra and smooth the values according to equation (3). The output will be compatible with the output of the PREDICT program. The user invokes this program by typing

\$RUN STAIN

#### A.1.5 SANDREF

The SANDREF program will model sand given the predicted transmittance and reflectance files (i.e., outputs from PREDICT, OPAQUE, and STAIN) of the constituent minerals, the sand configuration (e.g., particle size), and the sensing configuration. The user invokes this program by typing

\$RUN SANDREF

The user will be prompted for an output file which will contain the predicted reflectance spectrum. The user will then be prompted for an input file. The input file will contain the names of the files containing the predicted transmittances and reflectances which will make up the sand. The file will also contain a series of namelists which will describe various experimental configurations of sand composition and illumination-sensor geometries. Table A.1 defines these parameters and Table A.2 gives an example of the input file. The data for Quartz is defined as 90.2% transmittance and 9.8% reflectance over all wavelengths. Therefore if Quartz is listed as a mineral file, a file need not exist and the program will assign the above values. The user will also be prompted as to plotting the reflectance spectrum for the sand.

Table A.1. SANDREF Input Parameter Definitions

NMIN: Number of minerals in sand  
 NGEOM: Number of geometry namelists  
 X(1): Depth of top layer of sand (negative number)  
 X(2): Depth of bottom layer of sand (negative number)  
 PHI(1)-PHI(6): Polar view angles  
 TH: Sun (illuminator) angle  
 PSI(1)-PSI(7): Asimuth view angles  
 NAZ: Number of azimuth view angles  
 NPOL: Number of polar view angles  
 S(1,1,1)-S(2,2,6): H&V values for minerals

definition:  $H = \sigma'n$        $V = 1.414*H$

the array storage for S(I, J, K) is defined by

		1		2	
		I	J	I	J
Minerals	K				
	1				
	2				
	3	H	V	H	V
	4				
	5				
	6				
		Top Layer		Bottom Layer	

NSKY: = 0 if no sky (direct sun)  
       = 1 if sky (diffuse illumination)

Table A.2. Example of SANDREF Input File

```

1      1,      (NMIN)
2      MINI.35      (MINERAL FILE)
3      HF( AT=0.(1,303)      (BACKGROUND FILE)
4      0,      (NGEOM)
5      CARR 100%
6      RGEOM
7      X=-5.,-10.,PHI=7.,7.,7.,7.,7.,7.,TH=7.,PSI=90.,90.,90.,90.,90.,90.,
8      NAZ=1,NPOL=1,S=10.66,1.0,10.66,1.0,0,0,0,0,0,0,0,0,
9      0.,0.,0.,0.,0.,0.,0.,0.,0.,0.,0.,0.,NSKY=1,
10     REFD
11     CARR 100%
12     RGEOM
13     X=-5.,-10.,PHI=7.,7.,7.,7.,7.,7.,TH=7.,PSI=90.,90.,90.,90.,90.,90.,
14     NAZ=1,NPOL=1,S=5.66,1.0,5.66,1.0,0,0,0,0,0,0,0,0,
15     0.,0.,0.,0.,0.,0.,0.,0.,0.,0.,0.,0.,NSKY=1,
16     REFD
17     CARR 100%
18     RGEOM
19     X=-5.,-10.,PHI=7.,7.,7.,7.,7.,7.,TH=7.,PSI=90.,90.,90.,90.,90.,90.,
20     NAZ=1,NPOL=1,S=2.83,1.0,2.83,1.0,0,0,0,0,0,0,0,0,
21     0.,0.,0.,0.,0.,0.,0.,0.,0.,0.,0.,0.,NSKY=1,
22     REFD
23     CARR 100%
24     RGEOM
25     X=-5.,-10.,PHI=7.,7.,7.,7.,7.,7.,TH=7.,PSI=90.,90.,90.,90.,90.,90.,
26     NAZ=1,NPOL=1,S=2.83,.5,2.83,.5,0,0,0,0,0,0,0,0,
27     0.,0.,0.,0.,0.,0.,0.,0.,0.,0.,0.,0.,NSKY=1,
28     REFD
END OF FILE

```

BEST AVAILABLE COPY

REPRESENTATIVE OUTPUT SAMPLES  
FROM PROGRAMS



FORMERLY WILLOW RUN LABORATORIES, THE UNIVERSITY OF MICHIGAN

MINERAL :		CARBONATE *		
THICKNESSES :		0.05	0.35	0.23
SAMPLE NO.'S :		10047	30028	30179
		10024	30021	30152
WAVELENGTH	A	15	S	STD. DEVIATION
				OF
MICROMETERS	PER MILLIMETER	PER MILLIMETER		OF SPECTRAL FIT
0.35	1.25	0.05	15.86	0.03
0.36	1.07	0.11	16.48	0.03
0.37	0.93	0.05	16.02	0.03
0.38	0.81	0.03	15.87	0.03
0.39	0.69	0.14	16.76	0.03
0.40	0.62	0.08	16.64	0.04
0.41	0.55	0.06	16.63	0.04
0.42	0.49	0.01	16.33	0.04
0.43	0.43	0.01	16.39	0.04
0.44	0.39	0.01	16.42	0.04
0.45	0.35	0.01	16.57	0.04
0.46	0.32	0.01	16.68	0.05
0.47	0.29	0.01	16.61	0.05
0.48	0.27	0.01	16.46	0.05
0.49	0.25	0.01	16.60	0.05
0.50	0.23	0.01	16.61	0.05
0.51	0.21	0.01	16.61	0.05
0.52	0.19	0.01	16.39	0.05
0.53	0.18	0.01	16.67	0.05
0.54	0.17	0.01	16.10	0.05
0.55	0.15	0.01	15.61	0.05
0.56	0.14	0.01	15.53	0.05
0.57	0.13	0.01	15.46	0.06
0.58	0.12	0.01	15.58	0.06
0.59	0.12	0.01	15.27	0.06
0.60	0.11	0.01	15.66	0.06
0.61	0.10	0.01	14.49	0.07
0.62	0.10	0.01	15.16	0.06
0.63	0.09	0.01	15.07	0.06
0.64	0.09	0.01	14.83	0.07
0.65	0.08	0.01	14.49	0.07
0.66	0.08	0.01	14.52	0.07
0.67	0.08	0.01	14.57	0.07
0.68	0.07	0.01	14.73	0.07
0.69	0.07	0.01	14.05	0.07

BEST AVAILABLE COPY

Output from ABSCAT  
Input to PREDICT



FORMERLY WILLOW RUN LABORATORIES, THE UNIVERSITY OF MICHIGAN

MINERAL : CARBONATE \*

THICKNESS : 0.38 MM

WAVELENGTH  
(MICROMETERS)TRANSMITTANCE  
(PERCENT)REFLECTANCE  
(PERCENT)

0.35	1.11	30.61
0.36	1.45	37.99
0.37	1.80	40.65
0.38	2.23	41.96
0.39	2.94	43.85
0.40	3.18	45.60
0.41	3.64	47.61
0.42	4.08	49.36
0.43	4.73	51.18
0.44	5.25	52.51
0.45	5.79	54.06
0.46	6.25	55.32
0.47	6.89	56.51
0.48	7.43	57.29
0.49	7.83	58.35
0.50	8.35	59.37
0.51	8.94	60.41
0.52	9.74	61.46
0.53	10.34	61.75
0.54	10.68	62.38
0.55	11.90	63.26
0.56	12.41	63.88
0.57	12.94	64.54
0.58	13.32	65.46
0.59	13.61	65.12
0.60	13.77	66.26
0.61	15.47	65.95
0.62	14.79	66.61
0.63	15.47	67.38
0.64	15.71	67.11
0.65	16.70	67.69
0.66	16.99	67.72
0.67	16.61	67.77
0.68	17.10	68.86
0.69	17.35	68.15

Output from PREDICT  
Input to SANDREF

BEST AVAILABLE COPY

MINERAL : ILMENITE THICKNESS : 2.95 MM		
WAVELENGTH (MICROMETERS)	TRANSMITTANCE (PERCENT)	REFLECTANCE (PERCENT)
0.35	0.0	14.61
0.36	0.0	14.54
0.37	0.0	14.48
0.38	0.0	14.41
0.39	0.0	14.35
0.40	0.0	14.30
0.41	0.0	14.25
0.42	0.0	14.20
0.43	0.0	14.17
0.44	0.0	14.14
0.45	0.0	14.11
0.46	0.0	14.08
0.47	0.0	14.04
0.48	0.0	13.98
0.49	0.0	13.92
0.50	0.0	13.85
0.51	0.0	13.78
0.52	0.0	13.72
0.53	0.0	13.68
0.54	0.0	13.64
0.55	0.0	13.62
0.56	0.0	13.61
0.57	0.0	13.60
0.58	0.0	13.60
0.59	0.0	13.59
0.60	0.0	13.58
0.61	0.0	13.58
0.62	0.0	13.57
0.63	0.0	13.58
0.64	0.0	13.58
0.65	0.0	13.58
0.66	0.0	13.57
0.67	0.0	13.50
0.68	0.0	13.54
0.69	0.0	13.12

Output from OPAQUE  
Input to SANDREF



FORMERLY WILLOW RUN LABORATORIES, THE UNIVERSITY OF MICHIGAN

MINERAL : TRINITITE		
THICKNESS : 0.30 mm		
WAVELENGTH (MICROMETERS)	TRANSMITTANCE (PERCENT)	REFLECTANCE (PERCENT)
0.35	0.00	0.00
0.36	0.00	0.00
0.37	0.00	0.00
0.38	0.00	0.00
0.39	0.00	0.00
0.40	0.00	0.00
0.41	0.12	0.00
0.42	1.15	0.00
0.43	2.29	0.90
0.44	3.25	1.23
0.45	4.31	2.98
0.46	4.36	3.97
0.47	5.41	4.32
0.48	6.24	5.09
0.49	7.93	7.41
0.50	8.83	8.79
0.51	10.38	10.96
0.52	12.49	13.92
0.53	15.05	17.50
0.54	17.90	21.31
0.55	20.72	24.92
0.56	23.22	28.03
0.57	25.36	30.48
0.58	27.09	32.23
0.59	28.36	33.29
0.60	29.25	33.85
0.61	29.96	34.08
0.62	30.62	34.13
0.63	31.29	34.11
0.64	32.00	34.13
0.65	32.76	34.22
0.66	33.56	34.40
0.67	34.02	34.70
0.68	33.85	35.17
0.69	33.43	35.81

Output from STAIN  
Input to SANDREF

# REFERENCES

1. F. Thomson, R. Shuchman, C. Wezernak, D. Lyzenga and D. Leu, "Basic Remote Sensing Investigation for Beach Reconnaissance", Report 108900-5-P, Environmental Research Institute of Michigan, Ann Arbor, Michigan, July 1976.
2. G. Suits, "The Calculation of the Directional Reflectance of a Vegetative Canopy", Remote Sensing of Environment, Vol 2, pp 117-125, 1972.
3. R. E. Turner, "Radiative Transfer in Real Atmospheres", Report No. 190100-24-T, Environmental Research Institute of Michigan, Ann Arbor, 1974.
4. L. Elterman, "Vertical-Attenuation Model with Eight Surface Meteorological Ranges 2 to 13 kilometers", Report No. AFCRL-70-0200, Air Force Cambridge Research Laboratories, Bedford, Mass., 1970.
5. R. W. Austin, "Inherent Spectral Radiance Signatures of the Ocean Surface", in Ocean Color Analysis, Technical Report No. 74-10, Scripps Institution of Oceanography, San Diego, CA., 1974.
6. H. R. Gordon, D. B. Brown, and M.M. Jacobs, "Computed Relationships Between the Inherent and Apparent Optical Properties of a Flat Homogeneous Ocean", Applied Optics 14, 417 (1975).
7. D. R. Lyzenga, "Reflectance of a Flat Ocean in the Limit of Zero Water Depth", Applied Optics 16, 282 (1977).
8. N. G. Jerlov, Optical Oceanography, Elsevier Publishing Company, New York, 1968.
9. T. J. Petzold, "Volume Scattering Functions for Selected Ocean Waters," Visibility Laboratory Technical Report No. 72-78, Scripps Institution of Oceanography, San Diego, CA., 1972.
10. D. Deirmendjian, "Electromagnetic Scattering on Spherical Polydispersions", Elsevier Publishing Company., New York, 1969.
11. D. Lyzenga and F. Thomson, "Data Processing and Evaluation for Panama City Coastal Survey", Report No. 121400-1-T, Environmental Research Institute of Michigan, Ann Arbor, 1976.



FORMERLY WILLOW RUN LABORATORIES, THE UNIVERSITY OF MICHIGAN

## DISTRIBUTION LIST

Office of Naval Research Geography Programs Code 462 Arlington, Virginia 22217	2 copies	ONR Scientific Liaison Group American Embassy - Room A-407 APO San Francisco 96503
Defense Documentation Center Cameron Station Alexandria, Virginia 22314	12 copies	Commander Naval Oceanographic Office Attention: Library Code 1600 Washington, D.C. 20374
Director, Naval Research Lab Attention: Technical Information Officer Washington, D.C. 20375	6 copies	Naval Oceanographic Office Code 3001 Washington, D.C. 20374
Director, Office of Naval Research Branch Office 1030 East Green Street Pasadena, California 91101		Chief of Naval Operations OP 987P1 Department of the Navy Washington, D.C. 20350
Director, Office of Naval Research Branch Office 536 South Clark Street Chicago, Illinois 60605		Oceanographer of the Navy Hoffman II Building 200 Stovall Street Alexandria, Virginia 22322
Director, Office of Naval Research Branch Office 495 Summer Street Boston, Massachusetts 02210		Naval Academy Library U.S. Naval Academy Annapolis, Maryland 21402
Commanding Officer Office of Naval Research Branch Office Box 39 FPO New York 09510		Commanding Officer Naval Coastal Systems Laboratory Panama City, Florida 32401
Chief of Naval Research Asst. for Marine Corps Matters Code 100M Office of Naval Research Arlington, Virginia 22217		Librarian Naval Intelligence Support Center 4301 Suitland Road Washington, D.C. 20390
NORDA Code 400 National Space Technology Laboratories Bay St. Louis, Mississippi 39520		Officer in Charge Environmental Research Prdctn. Felty. Naval Postgraduate School Monterey, California 93940
Office of Naval Research Operational Applications Division Code 200 Arlington, Virginia 22217		Commanding General Marine Corps Development and Educational Command Quantico, Virginia 22134
Office of Naval Research Scientific Liaison Officer Scripps Institution of Oceanography La Jolla, California 92093		Dr. A. L. Slafkosky Scientific Advisor Commandant of the Marine Corps Code MC-RD-1 Washington, D.C. 20380
Director, Naval Research Laboratory Attention: Library, Code 2628 Washington, D.C. 20375		Defense Intelligence Agency Central Reference Division Code RDS-3 Washington, D.C. 20301



FORMERLY WILLOW RUN LABORATORIES, THE UNIVERSITY OF MICHIGAN

Director  
Defense Mapping Topographic Center  
Attention: Code 50200  
Washington, D.C. 20315

Commanding Officer  
U.S. Army Engineering  
Topographic Laboratory  
Attention: ETL-ST  
Fort Belvoir, Virginia 22060

Chief, Wave Dynamics Division  
USAE-WES  
P.O. Box 631  
Vicksburg, Mississippi 39180

National Oceanographic Data  
Center D764  
Environmental Data Services  
NOAA  
Washington, D.C. 20235

Central Intelligence Agency  
Attention: OCR/DD-Publications  
Washington, D.C. 20505

Dr. Mark M. Macomber  
Advanced Technology Division  
Defense Mapping Agency  
Naval Observatory  
Washington, D.C. 20390

Ministerial Direktor Dr. F. Wever  
RUE/FO  
Bundesministerium der Verteidigung  
Hardthoehe  
D-5300 Bonn, West Germany

Oberregierungsrat Dr. Ullrich  
Rue/FO  
Bundesministerium der Verteidigung  
Hardthoehe  
D-5300 Bonn, West Germany

Mr. Tage Strarup  
Defence Research Establishment  
Osterbrogades Kaserne  
DK-2100 Koberhavn O, Denmark

IR. M. W. Van Batenberg  
Physisch Laboratorium INO  
Oude Wallsdorper Weg 63, Den Haag  
Netherlands

Dr. Gordon E. Carlson  
University of Missouri  
Department of Electrical Engineering  
Rolla, Missouri 65401

Coastal Studies Institute  
Louisiana State University  
Baton Rouge, Louisiana 70803

Dr. Bernard Le Mehaute  
Tetra Tech. Inc.  
630 North Rosemead Boulevard  
Pasadena, California 91107

Dr. William S. Gaither  
Dean, College of Marine Studies  
Robinson Hall  
University of Delaware  
Newark, Delaware 19711

Dr. Lester A. Gerhardt  
Rennselaer Polytechnic Institute  
Troy, New York 12181

Mr. Fred Thomson  
Environmental Research Institute of Michigan  
P. O. Box 8618  
Ann Arbor, Michigan 48107

Dr. J. A. Dracup  
Environmental Dynamics, Inc.  
1609 Westwood Boulevard, Suite 202  
Los Angeles, California 90024

Dr. Thomas K. Peucker  
Simon Fraser University  
Department of Geography  
Burnaby 2, B.C., Canada

Dr. Bruce Hayden  
Department of Environmental Sciences  
University of Virginia  
Charlottesville, Virginia 22903